

COLOUR CENTRES IN ALKALI METAL AZIDES

by

JOHN PETER SCOTT PRINGLE

B.A. Cantab., 1956

A THESIS SUBMITTED IN PARTIAL FULFILMENT OF  
THE REQUIREMENTS FOR THE DEGREE OF

MASTER OF SCIENCE

in the Department

of

Chemistry

We accept this thesis as conforming to the  
required standard

THE UNIVERSITY OF BRITISH COLUMBIA

DECEMBER 1958

## Abstract

Previous work by Heal had shown that X-irradiated sodium azide crystals dissolved in water produced small amounts of nitrogen gas, hydroxyl ion and ammonia, thereby indicating that some decomposition had occurred. Heal also observed colours in the material, similar to those of the X-irradiated alkali halides for which a whole series of colour centres responsible have been postulated. It was therefore decided to investigate the colour centres of the alkali azides, partly to extend the colour centre research, and partly to illuminate the X-ray decomposition processes.

Crystalline plates of  $\text{NaN}_3$ ,  $\text{KN}_3$ ,  $\text{RbN}_3$  and  $\text{CsN}_3$  were irradiated at liquid nitrogen and room temperature, using a Machlett AEG-50 tungsten target X-ray tube, operated at 50 KVP. The absorption spectra of the irradiated samples were measured at liquid nitrogen temperature with a Cary model 14 recording spectrophotometer.

The low temperature spectra consisted of three bands.

The A band, peaking at 612, 568, 578 and 592  $\mu$  for  $\text{NaN}_3$ ,  $\text{KN}_3$ ,  $\text{RbN}_3$  and  $\text{CsN}_3$ , respectively, is ascribed to F centres. The anomalous sodium azide band is related to its trigonal crystal structure, differing from the body centred tetragonal of the other azides.

The B band, peaking at 361, 374 and 390  $\mu$  for  $\text{KN}_3$ ,  $\text{RbN}_3$  and  $\text{CsN}_3$  respectively, was strong and triple, there being shoulders about 30  $\mu$  on each side of the main peak. For  $\text{NaN}_3$  it was weak, single and peaked near 330  $\mu$ . Tentatively, it is ascribed to the  $V_1$  centre.

The C band, peaking about 740, 790, 820 and 850  $\mu$  for  $\text{NaN}_3$ ,  $\text{KN}_3$ ,  $\text{RbN}_3$  and  $\text{CsN}_3$  is weak and single. It may be due to  $F'$  centres.

The room temperature spectra were strikingly different from each other, except for  $\text{RbN}_3$  and  $\text{CsN}_3$ .

For  $\text{NaN}_3$  five bands were observed at 342, 560, 630, 730 and 860  $\mu$ ; the latter four were weak and may be an electronic vibrational spectrum. The strong 342  $\mu$  band is ascribed to the presence of sodium metal in some non-colloidal form; a correlation between the band and the ionisation potential of the metal is noted.

In  $\text{KN}_3$  three bands at 760 (strong), 590 (strong shoulder) and 340  $\mu$  (weak) were obtained. The first two are ascribed to small F centre aggregates of the  $M_2R$  type though no definite assignments are made.

$\text{RBN}_3$  and  $\text{CsN}_3$  spectra both consist of a broad peak showing fine structure, the highest peaks occurring at 330  $\mu$  and 375  $\mu$  respectively. It is considered uncertain that all the absorption is due to the impurity held responsible for the fine structure.

In presenting this thesis in partial fulfilment of the requirements for an advanced degree at the University of British Columbia, I agree that the Library shall make it freely available for reference and study. I further agree that permission for extensive copying of this thesis for scholarly purposes may be granted by the Head of my Department or by his representative. It is understood that copying or publication of this thesis for financial gain shall not be allowed without my written permission.

Department of Chemistry

The University of British Columbia,  
Vancouver 8, Canada.

Date 24<sup>th</sup> December 1958

## TABLE OF CONTENTS

	<u>Page</u>
Introduction.	1
Experimental methods.	3
1. Preparation of samples.	3
2. Analysis of samples.	5
3. Irradiation cell.	7
4. X-ray tube circuit.	8
5. Production of X-rays.	9
6. Filtration and absorption of X-rays.	9
7. Spectrophotometric technique.	11
Discussion.	14
1. Effects of X-rays on solids.	14
2. Imperfections in ionic solids.	15
3. Colour centres in alkali halides.	17
(i) F centres	17
(ii) F' centres.	18
(iii) R <sub>1</sub> , R <sub>2</sub> , M and N bands.	19
(iv) Colloidal bands.	19
(v) V bands.	19
(vi) Miscellaneous bands.	20
4. Crystal structures.	21
Results.	21
1. Processing of spectra.	21
2. Spectra of unirradiated azides.	22
(i) Spectra below absorption edge.	22
(ii) Spectra at absorption edge.	23

Results (cont'd)	<u>Page</u>
3. Spectra of azides irradiated at liquid nitrogen temperatures.	26
(i) A band.	26
(ii) B band.	30
(iii) C band.	33
4. Spectra of azides irradiated at room temperature.	33
(i) Sodium azide.	34
(ii) Potassium azide.	35
(iii) Rubidium and Caesium azides.	36
References.	38

Tables

Table I. Analysis of azides by Heal's Method.	6
Table II. Calculations on Exciton absorption bands.	24
Table III. Comparison of A and F bands.	27
Table IV. Comparison of B and $V_1$ bands.	31

TABLE OF FIGURES

<u>Figure No.</u>	<u>Page</u>
1. Irradiation cell.	7A
2. X-ray circuit.	8A
3. Filtration and absorption of 50 PKV X-rays.	9A
4. Mass absorption coefficients of azides and filters.	10A
5. Energy bands in ionic solids.	15A
6. Possible vacancies and vacancy aggregates in alkali halides.	15A
7. Edge dislocation in an alkali halide.	15A
8. Production of vacancies from an edge dislocation.	15A
9. Colour centres in alkali halides: Seitz (16).	17A
10. Crystal structures of (a) $\text{NaN}_3$ and (b) $\text{KN}_3$ .	17A
11. Four spectra of unirradiated $\text{NaN}_3$ .	17A
12. Unirradiated azide spectra below absorption edge.	23A
13. Absorption edge spectra, (a) present work and (b) reference (9)	23A
14. $\text{NaN}_3$ irradiated at liquid nitrogen temperature.	26A
15. $\text{KN}_3$ irradiated at liquid nitrogen temperature.	26B
16. $\text{RbN}_3$ irradiated at liquid nitrogen temperature.	26C
17. $\text{CsN}_3$ irradiated at liquid nitrogen temperature.	26D
18. "C" band spectra of $\text{KN}_3$ , $\text{RbN}_3$ and $\text{CsN}_3$ .	33A
19. Irradiated $\text{NaN}_3$ spectra at room temperature.	34A
20. Irradiated $\text{KN}_3$ spectra at room temperature.	35A
21. Irradiated $\text{RbN}_3$ and $\text{CsN}_3$ spectra at room temperature.	36A

## Introduction

The study of the chemical effects produced in matter by radiations can be conveniently divided into two fields, photochemistry and radiation chemistry. In photochemistry, the (electromagnetic) radiation energy is of the same order as that of the electrons involved in normal chemical bonding i.e. less than 10 eV; the absorption of such energy results in a single electronic excitation or, more rarely, a single ionisation, as the primary event. The much higher energies of radiation chemistry are dissipated by a series of such primary processes, each incident particle or quantum being capable of producing multiple ionisations or excitations.

High energy radiations can be classified (1) into two types. The light particle group includes all those radiations transferring energy to the medium by means of fast electrons; beta and cathode rays where the electrons are produced externally, and gamma and X-rays in which the electrons are produced in the medium itself via the photoelectric or Compton effects, or pair production. Alpha particles, neutrons, fission products and accelerated ions form the heavy particle group; both groups produce broadly similar chemical effects.

The present work describes an investigation of X-radiation induced effects in alkali metal azides. Previous work by Heal (2,3) had shown that X-irradiated sodium azide evolved nitrogen gas on dissolution in water; the resulting solution contained appreciable amounts of hydroxyl ion and ammonia. Solution in liquid ammonia at  $-78^{\circ}\text{C}$  resulted in effervescence and a blue colour, indistinguishable from that of a similar solution of sodium metal; none of these results were reproduced with unirradiated samples, thereby showing that some decomposition had occurred. Similar ionic azide decomposi-

tions produced thermally (4,5,6) or by the action of ultra violet light (7,8,9) have been studied, and mechanisms proposed; recently Grocock and Tompkins (10) have studied the decomposition induced by electron bombardment.

Heal also observed colours produced by X-irradiation of the normally colourless sodium azide; an unstable pale green turning to brown in crystals irradiated at or below room temperature, a stable brown colour on irradiation between 51°C and 102°C, and a greyish or bluish tinge, together with loss of transparency and waxy appearance, in crystals irradiated above 130°C. The brown colour was ascribed by Heal to the tail of an absorption band peaking at 3400Å, a band confirmed by the work of Rosenwasser, Dreyfus and Levy (11), who placed it at 3600Å. The latter group, using sodium azide irradiated in the Brookhaven reactor followed by various heat treatments, obtained five other absorption bands in the range 2700Å to 12000Å. A similar series of absorption bands was found by Tompkins and Young (12) in potassium azide irradiated with ultraviolet light.

The colours produced by X-irradiation of the alkali halides have long been known (13), and the absorption bands responsible have been extensively investigated; reviews of this field have been given by Pohl (14), and Seitz (15,16). A whole series of "colour centres" have been postulated to account for the absorption bands; these will be considered in a later section of the present work. In view of the similarities between the alkali halides and the alkali azides, it was considered that an investigation of the absorption bands produced by X-irradiation of the latter would be valuable; firstly, as an extension the "colour centre" research, and secondly, because it might indicate the decomposition mechanism in X-irradiated azides.

## Experimental Method

### 1. Preparation of Samples

(i) Hydrazoic acid required for the preparation of the potassium salt and to suppress hydrolysis in recrystallising solutions of the azides, was prepared by two methods. In the first, a column of the cation exchange resin, Dowex 50W - X-8 in the  $H^+$  form was set up, 125 cms. long by 2.4 cms. diameter; the total exchange capacity was about 1000 milli-equivalents. After washing with 500 ml. distilled water, 10 gms. of  $NaN_3$  practical grade, dissolved in 200 ml. distilled water, was passed through at the slow flow rate of 2.4 ml/sq.cm/minute, the eluting agent being more distilled water. It was observed that a deep red brown band with sharp lower and diffuse upper boundary formed near the top of the column on addition of the  $NaN_3$  solution; this band moved slowly down the column as elution proceeded, vanishing shortly after the last of the  $NaN_3$  had been added, in a position corresponding roughly to the number of milli-equivalents of  $Na^+$  used. In the latter stages, a faint brownish colour appeared below the band and eluted with the  $HN_3$ ; while the resin above the band, presumably in the  $Na^+$  form, became more orange in colour and contracted in volume, an effect indicated by the makers. The hydrazoic acid obtained in this way was colourless but weak, barely 2% solutions being obtained; a small amount continued to elute long after the majority had come through. On dissolving sodium azide in this solution with intent to recrystallise, a yellow colour was observed; for this reason, and also because only weak  $HN_3$  solutions could be produced, the method was discontinued.

The second method used the procedure described in Inorganic Syntheses (17): 40%  $H_2SO_4$  was added slowly to a boiling solution of  $NaN_3$ , the  $HN_3$  distill-

ing off in the steam, being condensed and collecting in a receiver containing distilled water. A reddish colour was observed in the boiling solution on the initial addition of the acid; this is ascribed to impurities in the commercial sodium azide, probably  $\text{Fe}^{3+}$ , the effect of which was studied by El-Shami and Sherif (18). By reducing the quantities of water used,  $\text{HN}_3$  concentrations up to 5% were obtained.

- (ii) Sodium azide was obtained commercially from Eastman Kodak in practical grade, and recrystallised from 3% hydrogen azide solution using an oven switched off at  $90^\circ$  to provide slow cooling. Suitable transparent plates of thickness about 0.1 mm. and area up to 30 sq. mm. were obtained; such plates had small regular corrugations in the surfaces giving a feathery appearance by reflected light, but having no visible effect on transmitted light.
- (iii) Potassium azide was prepared by neutralising hydrogen azide with reagent grade potassium hydroxide. The solution was then concentrated and attempts made to recrystallise the material. Much difficulty was encountered in obtaining suitable plates; recrystallisation by the sodium azide method gave either irregular lumps or plates too small to be of use. More success was obtained by using some of the latter as seeds, laying them flat on the bottom of a beaker containing a hot saturated solution. Rather thick plates were obtained in this way, of area up to 45 sq. mm. and average thickness about 0.34 mm; the plates were also a good deal less transparent than those of the other azides.
- (iv) Rubidium azide was obtained from A. D. Mackay Inc. who stated it contained at least 1% potassium and a trace of caesium. It was recrystallised from distilled water under slow evaporation in a vacuum desiccator; excellent transparent plates of area up to 20 sq. mm. and thickness 0.3 mm. were obtained at the first attempt.

- (v) Cæsium Azide was also acquired from A.D. Mackay Inc. who indicated it was about 99.8% pure. Large transparent plates were obtained by recrystallising from hot distilled water; the area ranged to 40 sq. mm. and the thickness to 0.15 mm.
- (vi) Lithium, Strontium and Barium azides. Attempts were made to prepare the azides of lithium, barium and strontium as crystalline plates suitable for the measurement of absorption spectra. All were prepared by neutralising the oxide as hydroxide with excess hydrazoic acid. On concentrating the solutions, however, barium azide gave thick irregular needles, strontium azide opaque white deposits, and lithium azide came out <sup>of</sup> a very concentrated solution only when the whole mass turned into a brownish solid. The brown colour could be removed by successive washings in ethyl alcohol, in which the lithium azide was not soluble, contrary to the published figure of 20 gm/100 ml. EtOH quoted by Audrieth (19). After drying for several weeks in an oven at 90° C., analysis, by the method described below, showed the white powder to be very impure; it gave a strongly alkaline reaction in water from which it is inferred that the major impurity was hydroxide.

## 2. Analysis of Samples

The samples were analysed by the method of Heal (2). About 0.002 gram equivalent weight of azide (0.13 gm. for  $\text{NaN}_3$ , 0.35 gm. for  $\text{CsN}_3$ ) was weighed to the nearest 0.01 mg. in a 5 ml. Pyrex beaker. Two millilitres of normal HCl were then added to the beaker and the whole evaporated under an infra-red lamp almost to dryness, when two more millilitres of HCl were added. This time the system was evaporated carefully to complete dryness, followed by two more millilitres of HCl, making 0.006 gram equivalent weight of HCl added altogether; again the system was evaporated to complete dryness. The beaker and chloride were weighed to 0.01 mg. as before; the ratio chloride to azide was calculated

Table I. Analysis of azides by Heal's method (2)

Chloride: Azide ratios.

<u>Azide</u>	Starting Material	Samples Used	Theoretical value
NaN <sub>3</sub>	0.9091	0.9028	0.8990
	0.9056	0.9053	
	0.9088	0.9005	
KN <sub>3</sub>	0.9237	0.9196	0.9190
	0.9319	0.9177	
	0.9336		
RbN <sub>3</sub>	0.9506	0.9502	0.9485
	0.9472		
CsN <sub>3</sub>	0.9585	0.9630	0.9265
		0.9594	
LiN <sub>3</sub>	1.1114		0.8658
	1.1118		
	1.1125		
	1.1124		
Sr(N <sub>3</sub> ) <sub>2</sub>	0.9215		0.9235
	0.9182		
Ba(N <sub>3</sub> ) <sub>2</sub>	0.9399		0.9406
	0.9336		

and compared with the theoretical value. Table I shows the results obtained for the starting materials, the samples used and the theoretical values.

It is considered that the standard error of the balance is  $\pm 0.00004$  grams in the range used, 4-5 grams, and that the error in the resultant ratios attributable to this cause is about 0.001. The total errors in the ratios may be higher since it was rather difficult to avoid spitting as dryness was approached, though this could be reduced by moving the lamp further away. Attempts to precipitate the chlorides in finely divided form by adding two millilitres of acetone did not reduce the spitting.

The high values of the sodium ratios are ascribed to traces of water left in the sodium chloride on evaporation. According to Duval (20), NaCl does not attain constant weight below  $407^{\circ}\text{C}$ ; experiments with a thermocouple showed that under the normal conditions of evaporation in which one, two or three infra-red lamps were used the temperatures attained were about  $160^{\circ}\text{C}$ ,  $240^{\circ}\text{C}$  and  $310^{\circ}\text{C}$  respectively. This effect does not occur in the other chlorides since the constant weight temperatures are much lower;  $219^{\circ}\text{C}$  for KCl,  $88^{\circ}\text{C}$  for RbCl and  $110^{\circ}\text{C}$  for CsCl.

### 3. Irradiation cell

The irradiation cell used is depicted in figure I. The sample, in the form of a crystalline plate, was cemented with label varnish across a hole, 3 or 4 mm. square depending on the size of the crystal, in the slotted copper block, which in turn was screwed to the bottom of the metal dewar. The cell was evacuated by connecting the metal flange on the right of the brass vacuum valve to a similar flange attached to an evacuation train, consisting of mechanical fore pump, mercury diffusion pump, liquid air trap and Pirani gauge. The temperature of the sample was controlled by putting an appropriate coolant in the dewar, and measured with the aid of a thermocouple.

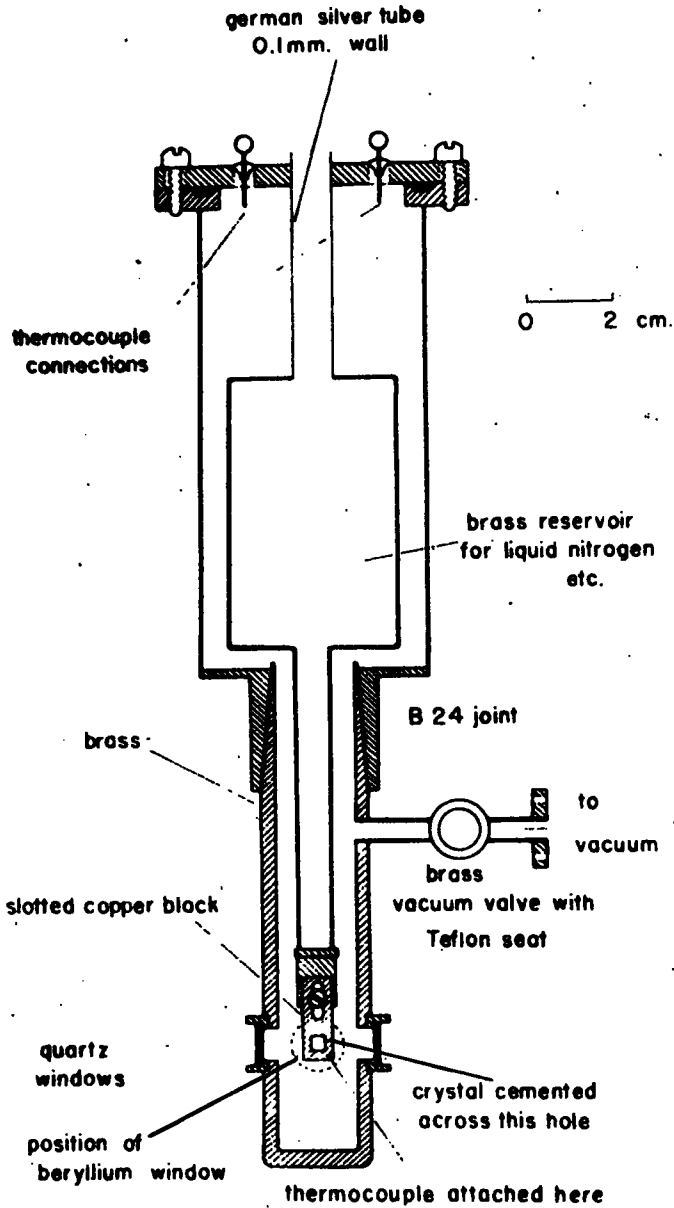


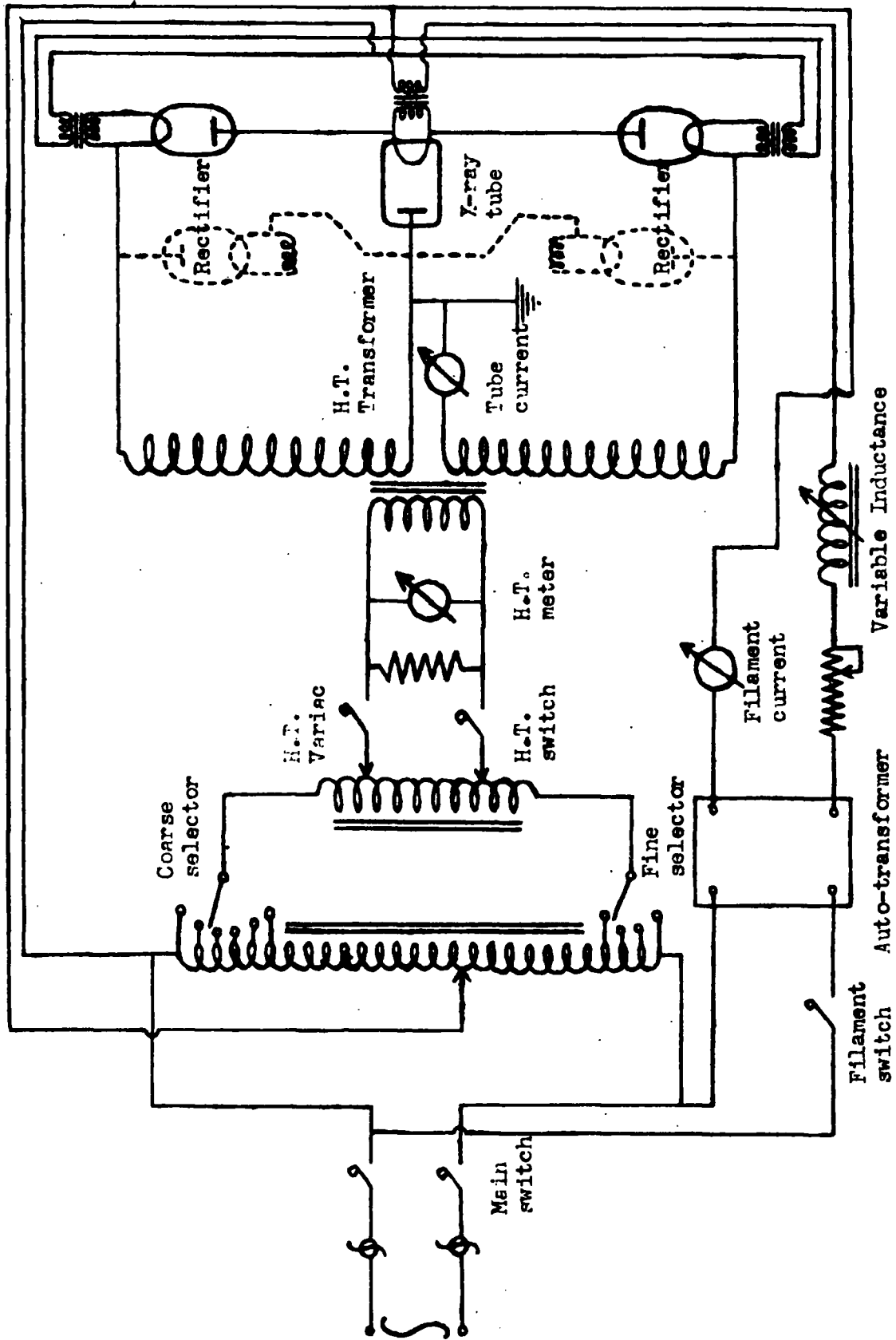
Fig. 1. Irradiation cell.

To irradiate the sample was turned parallel to the beryllium window by rotating the top of the cell about the B24 joint until two marks, one on each half of the joint, coincided. Absorption spectra were taken by rotating the cell through  $90^\circ$ , as measured by another mark on the joint so that the crystal became parallel to and in line with, the quartz windows through which the spectrophotometer beam passed. The cell could be attached to the port of the X-ray tube or placed in the cell compartment of the Cary Model 14 spectrophotometer, by arrangements not shown in the diagram.

#### 4. X-ray tube circuit

Figure 2 gives the circuit supplying power to the non-shockproof Machlett AEG-50 type T X-ray tube. The circuit is essentially a General Electric X-ray unit giving full wave rectification, modified by the removal of two of the rectifier tubes, shown dotted in the figure, to give an output voltage of 50 KVP instead of 100 KVP; the spare high voltage terminal was grounded. The modification also had the property of doubling the current obtainable, which was limited by the heat generated in the transformer. The voltage across the X-ray tube was controlled by means of the H.T. Variac, and measured by the meter in the H.T. primary circuit. An auto transformer was placed in the circuit of the X-ray filament supply to stabilise the filament current, on which the tube current markedly depends. This dependence was used to control the tube current by means of the variable inductor in the filament circuit; the tube current was measured by means of a meter in the grounded anode circuit, whose readings had to be doubled since it operated only on one half of the cycle. Certain relays, incorporated as safety devices, are not shown in the diagram; a water switch was placed in the cooling water supply to the anode, which cut off the H.T. when the flow rate was too low.

Fig. 2. X-ray circuit (Heal, private communication).



## 5. Production of X-rays

The X-irradiation used in this work was obtained from a non-shockproof Machlett AEG-50 Type T X-ray tube, equipped with a water cooled tungsten target. Such tubes have a maximum power rating for continuous use of 50 milliamperes at 50 KVP; in practice, the tube was run at 50 KVP and 28 milliamperes or less. A  $44^\circ$  cone of X-rays is emitted through a 1 mm. thick beryllium window; the energy distribution of the continuous X-ray spectrum was calculated with the aid of De Waard's formula (21) and is shown in figure 3. It can be seen that there is a steep rise at the short wave lengths, starting from the critical wavelength at  $0.248\text{\AA}$ , which corresponds to the total energy of a 50 KV electron.

Peak energy occurs at about  $0.440\text{\AA}$  and there is a pronounced tail at the longer wave lengths. The voltage used was insufficient to excite the characteristic K emission lines of tungsten, which requires at least 69 KV; and the intensity of the L lines is considered by Heal (22) to be negligible.

## 6. Filtration and Absorption of X-rays

The X-ray absorption due to any element increases with the atomic number, and also with the wavelength of the incident radiation, except at absorption edges, where there is a discontinuous change. In a given system, it depends only on the number of atoms of that element present, and not at all on their chemical and physical environment. These properties make it possible to measure a mass absorption coefficient for each element, which can then be suitably added together to give the mass absorption coefficients of compounds or mixtures. The mass absorption coefficients have not been measured for all elements, but their variation is sufficiently well known to enable Victoreen (23) to produce empirical formulas for calculating them, which agree, so he claims, to within 1% of the best average measured values; the experimental values being somewhat variable.

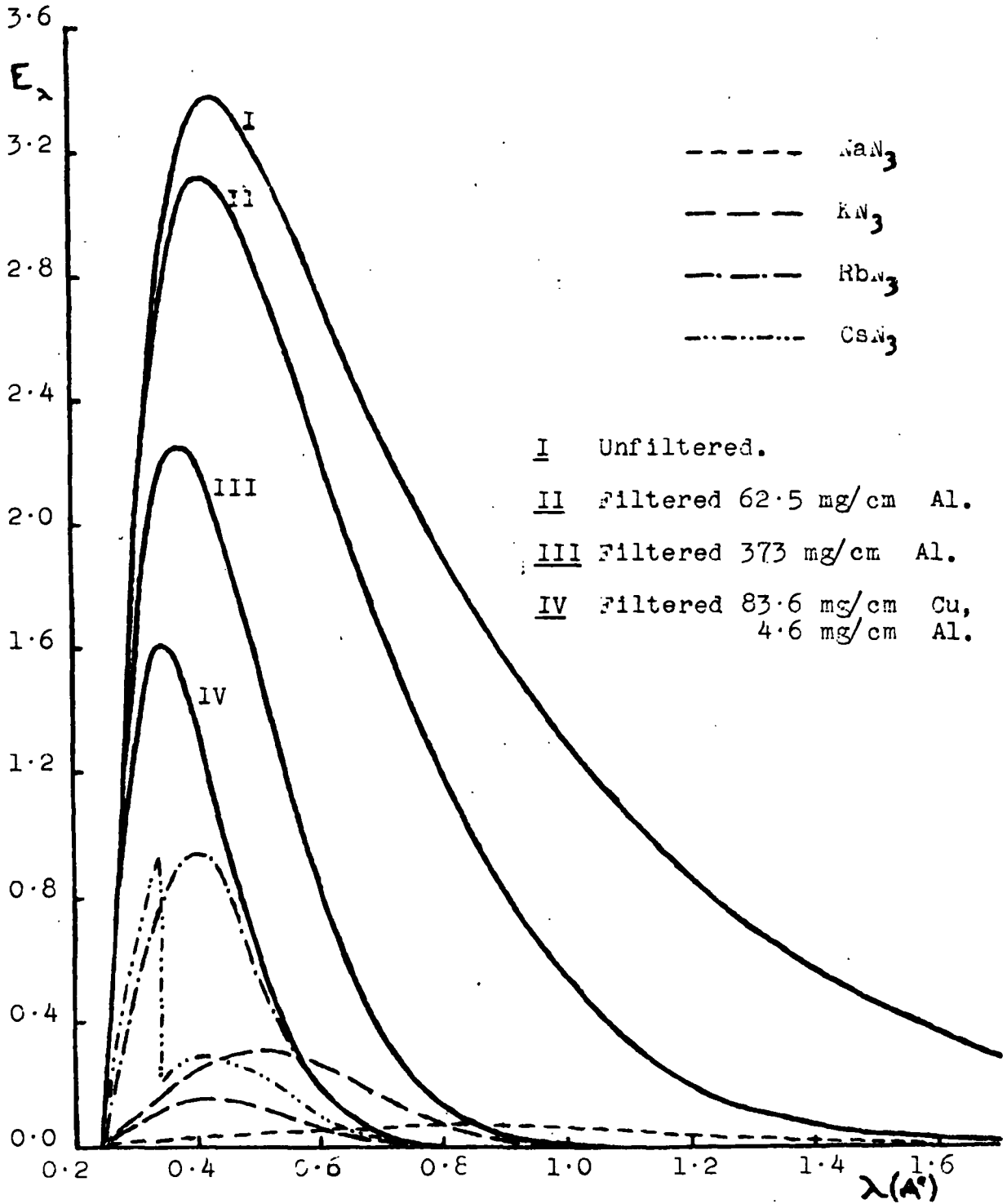


Fig. 3. Filtration and absorption of 50PKV X-rays.

Using Victoreen's formulas the specific absorption coefficients of the azides have been calculated and are plotted in Figure 4, together with data for aluminium and copper.

The higher the specific absorption the more the X-ray beam is absorbed in the surface layers of the material relative to the bulk. In order to obtain reasonably uniform irradiation, therefore, it was desirable to reduce the intensity of the longer wavelengths at which the specific absorption coefficients are high. This was done by interposing metal foils in the path of the X-ray beam; figure 3 shows the spectral distribution of the X-radiation after filtration by a) 62.5 milligrams per square centimetre of aluminium, used for  $\text{NaN}_3$ , b) 373 milligrams per square centimetre of aluminium used for some  $\text{KN}_3$  runs, and c) 83.6 milligrams per square centimetre of copper and 4.6 milligrams per square centimetre of aluminium, used for  $\text{KN}_3$ ,  $\text{RbN}_3$ , and  $\text{CsN}_3$ . The attenuation of the X-ray beam at any wavelength was calculated from the Beer-Lambert law:

$$I_{\lambda} = I_{\lambda}^0 e^{-\mu_{\lambda} x} \quad \text{where } I_{\lambda}^0, I_{\lambda} \text{ are the incident and emergent intensities respectively, } \mu_{\lambda} \text{ is the linear absorption coefficient at wavelength } \lambda \text{ and } x \text{ is the thickness of the sample. For the purposes of calculation, this formula was modified to:}$$

where  $\left(\frac{\mu_{\lambda}}{\rho}\right)$  is the mass absorption coefficient and  $\rho x$  is expressed in grams per square centimetre,  $\rho$  being the density of the material.

$$I_{\lambda} = I_{\lambda}^0 e^{-\left(\frac{\mu_{\lambda}}{\rho}\right)(\rho x)}$$

Similar calculations were performed to find the fraction of the incident X-ray energy absorbed by the azide samples, which is proportional to  $1 - e^{-\left(\frac{\mu_{\lambda}}{\rho}\right)(\rho x)}$ . It varies with the wavelength, and, multiplied by  $I_{\lambda}^0$ , has also been plotted in figure 3. As an approximation to uniform irradiation throughout the crystals, it was considered by Heal advisable to keep the fraction of the incident X-ray energy absorbed below 10%. This was not possible for  $\text{KN}_3$ ,  $\text{RbN}_3$ , or  $\text{CsN}_3$  because

Similar calculations were performed to find the fraction of the incident X-ray energy absorbed by the azide samples, which is proportional to  $1 - e^{-\left(\frac{\mu_{\lambda}}{\rho}\right)(\rho x)}$ . It varies with the wavelength, and, multiplied by  $I_{\lambda}^0$ , has also been plotted in figure 3. As an approximation to uniform irradiation throughout the crystals, it was considered by Heal advisable to keep the fraction of the incident X-ray energy absorbed below 10%. This was not possible for  $\text{KN}_3$ ,  $\text{RbN}_3$ , or  $\text{CsN}_3$  because

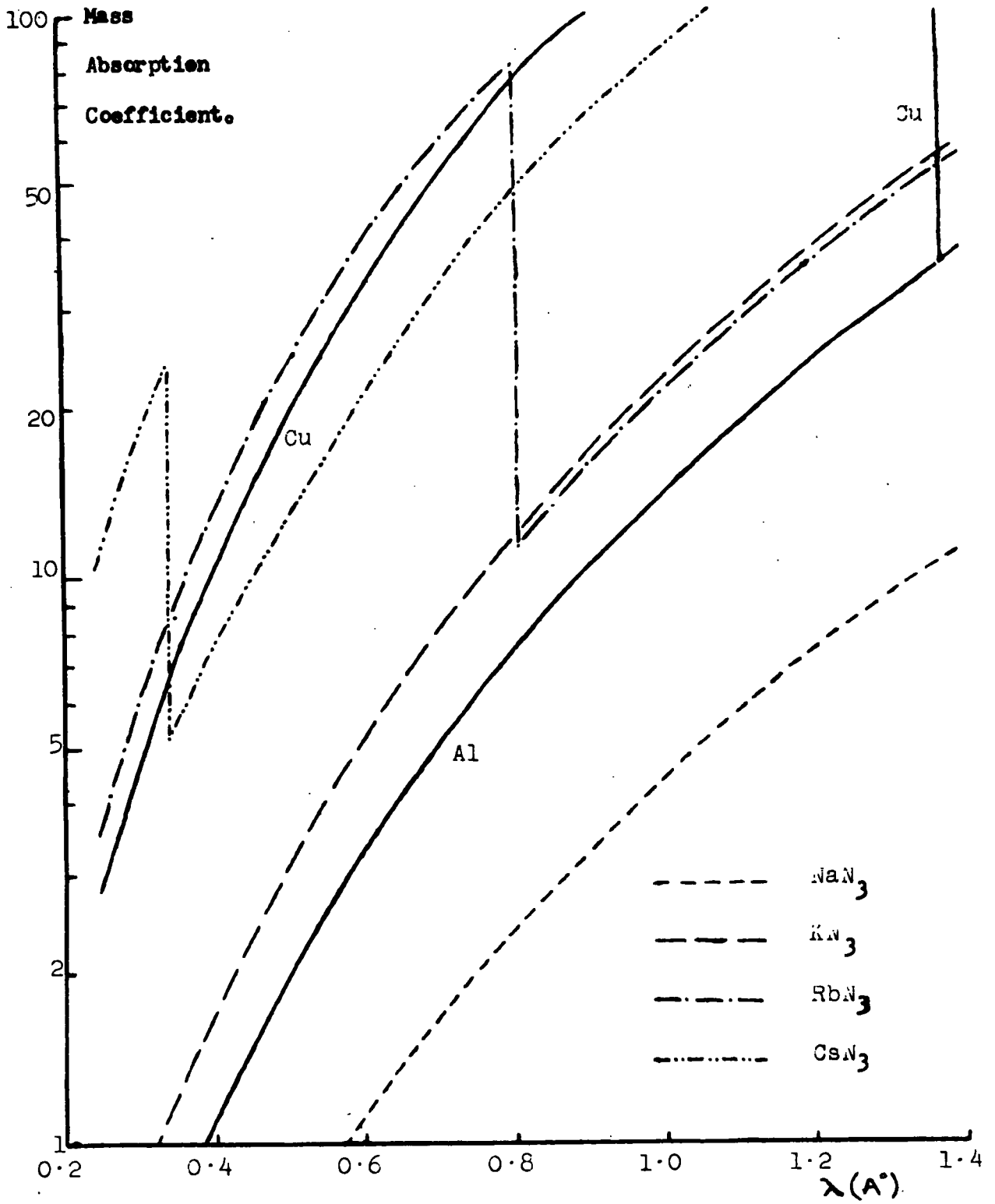


Fig. 4. Mass absorption coefficients of azides and filters.

the fraction of the incident energy absorbed depends on the quantity  $\left(\frac{\mu}{\rho}\right)(\rho x)$ ;  $\left(\frac{\mu}{\rho}\right)$  and  $\rho$  are fixed quantities, while  $x$  is fixed for a given crystal, and was far too large in the cases quoted. The quantity  $\rho x$  was determined for the azide samples from the area of the crystals, estimated by laying them flat on graph paper, and their weight as measured on a Cahn electro-balance.

## 7. Spectrophotometric technique

### (i) Characteristics of wavelength regions

The Cary model 14 spectrophotometer used covers the wavelength region from 26000A° to 2000A°, in three ranges, referred to as "IR", "VIS" and "UV".

The "VIS" region covers the range of wavelengths from about 8200A° to 2900A°, though the useful range extends only from about 7400A° to 3200A°; below 3200A° the slit width varies rather rapidly, while above 7400A° there appears to be a drop in the response of the IP28 photo-tube detector. The spectrum is obtained from an ordinary General Electric projection lamp, and analysed into its wavelength components by successive passage through a prism and diffraction grating; the monochromatic beam produced passes through a slit, and the sample into the detector.

The "UV" region uses a hydrogen discharge lamp, but the optical path is otherwise similar to that of the "VIS" region; it was used from 3500A° down to about 2500A°, at which point the first fundamental absorption band of the azides is reached.

In the "IR" region, which also uses a General Electric projection lamp, the optical path is reversed. The whole spectral range whose useful limits were 26000A° to 3500A°, passes through a slit and onto the sample; only then is it broken up into its components by the monochromator, and fed into the PbS detector.

This difference between the "IR" and "VIS" regions was of immense significance for absorption bands unstable to light, of which several were encountered in this work. Scanning over the "VIS" and "UV" ranges combined would take about ten minutes at the normal scanning speed of  $10\text{Å}^{\circ}/\text{sec.}$ ; under these conditions each wavelength would be incident on the sample for rather less than one second, since the resolving power of the monochromator is said to be  $1\text{Å}^{\circ}$  in these regions. The whole scanning operation therefore would have as much bleaching effect on the unstable absorption bands as under one second's work in the "IR" region, where all the wavelengths are incident on the sample all the time.

(ii) Characteristics of spectrophotometer beam

The Cary model 14 is a double beam type of spectrophotometer, the sample and reference beams passing through two separate compartments each about 10 cms. long in which apparatus can be placed. The beams are focused at the centre of these compartments, where they form a rectangular vertical image, and where the samples are placed in normal use. The size of the beams is controlled by a) the Slit Width control, automatically operated by the machine, which varies the slit width, and hence also the image width between 0 and 3 mm. as recorded on a meter; and b) the Slit Height control, which varies the slit height between 7 mm. and 20 mm. and whose function is to correct for mismatches of wavelengths by the monochromator at extreme range. According to the makers (24) the size of the image is 15.8 mm. by 3.15 mm; approximate measurements with a ruler in the "VIS" region with the slit wide open indicated that the actual size was nearer 12 mm. x 3 mm. or, with the slit height reduced to its full extent, 7 mm. x 3 mm. Since the maximum height of the beam emerging from the sample was only 4 mm., the size of the crystal aperture, the slit height control could have little effect, and was therefore invariably left open to its full extent.

(iii) Alignment of Crystals

The crystals were aligned with the spectrophotometer beam by means of a special carriage. The irradiation cell was screwed to a brass block, which was free to move along two vertical brass rods to which it could be screw clamped; this allowed the samples to be correctly aligned in a vertical direction. The brass rods were fastened to a horizontal aluminium tray resting on supports in the sample compartment; by means of a handle projecting outside the compartment the tray could be moved so that the samples were correctly aligned in a horizontal direction with respect to the beam. Horizontal alignment was invariably done at a wavelength near  $8000\text{\AA}$  on the "VIS" range, where the image width was nearly as wide as the sample itself, and was checked by minimising the absorption recorded.

(iv) Operational observations

At the start of the experiments, the samples were set by eye in the middle of the "VIS" beam. It was then discovered that, on changing to the "UV" beam at  $3500\text{\AA}$ , there was a discontinuous jump in the absorption and also that the slopes of the absorption curve were different in the two regions. This trouble was traced to the fact that the "UV" beam was not following an identical path to the "VIS", but was passing at a lower level; lowering the crystal reduced the effect substantially. Slight variations in recorded absorption were also observed in the region  $7400\text{\AA}$  to  $6000\text{\AA}$  where the "VIS" and "IR" regions overlapped; these are ascribed to a similar effect, and also the fact that the two beams were incident on opposite faces of the crystals.

It was observed that there was a marked gradation in intensity across the "UV" beam, and to a lesser extent in the "VIS" also.

An aluminium sheet with a hole bored in it of approximately the same size as that of the crystal holder, was placed in the reference beam to equalise the

size of the beams reaching the detectors. The hole was aligned with the "VIS" and "UV" beam by inspection.

## Discussion

### 1. Effects of X-irradiation on solids

The primary effect of the passage of X-irradiation through matter is the production of fast electrons by one of three processes. If the energy of the X-radiation is greater than one MeV, pair production is possible; this consists of the simultaneous production of a positron and an electron when the photon passes close to an atomic nucleus, and is the most probable process at very high energies. For lower energies, such as the 50 KeV used in the present work, fast electrons are produced either by the Compton effect or by the photoelectric effect. In the former, an X-ray photon interacts with an electron and is scattered, giving up part of its energy to the electron, and appearing as X-radiation of longer wavelength. The photoelectric effect occurs when all the energy of the incident photon is absorbed by an electron in an atomic inner orbital, resulting in the ejection of the electron from the atom. Calculations by Lea (25) show that for a 51 KeV X-ray quanta absorbed in water the proportion of primary photoelectrons is 0.151, the rest being Compton recoils; but the photoelectrons, being more energetic, are responsible for 0.684 of the total electron energy. The average primary electron energy is calculated to be about 15 KeV for this system.

The fast primary electrons produced lose energy in traversing matter because their rapidly moving charge perturbs the electronic system of the material, resulting in electronic excitation and ionization; such ionisation is frequently so vigorous that the secondary electron freed has sufficient energy ( $\sim 100\text{eV}$ ) to cause ionisation on its own account. In ionic solids, such as the azides, ionisation corresponds to the raising of an electron from the valence band into the conduction band, leaving a positive hole in the band from whence it came.

The production of excitons corresponds to the electronic excitation discussed above; an exciton, which is mobile in the lattice, can be considered as an electron bound to a positive hole in the same manner as it is bound to a proton in the hydrogen atom. Figure 5 is an energy diagram showing the transitions involved. It is the interaction of these conduction band electrons, excitons, and holes with the lattice defects described in the next section that produce the colour centres described in section 3.

## 2. Imperfection in ionic solids

The necessary existence of lattice imperfections was first pointed out by Frenkel, (26) who showed that the electrolytic conductivity observed in the alkali halides at high temperatures was not explicable in terms of a perfect ionic lattice; but required that a certain fraction of the ions be free to wander round the lattice. An applied electric field orients the motion, and results in the passage of the current.

In order to explain the free ions, Frenkel proposed that an ion could jump to an interstitial position (Frenkel defect) leaving a vacancy at the normal lattice site; the current could be carried either by the interstitial ion moving through the lattice, or by the vacancy travelling in the opposite direction through successive jumps of ions into it. Schottky (27) pointed out that the displaced ion could be added to the surface of the crystal instead of an interstitial position; thus leaving isolated vacancies (Schottky defects) which were perfectly capable of explaining the observed ionic conductivity and diffusion effects. Calculations by Mott and Littleton (28) indicate that interstitial ions are unlikely to occur in the alkali halides since the energy required for their formation is high. Thus in NaCl, an interstitial  $\text{Na}^+$  requires 2.9 eV for its formation, while a pair of separated vacancies requires only 1.9 eV; even at the melting point the number of interstitial

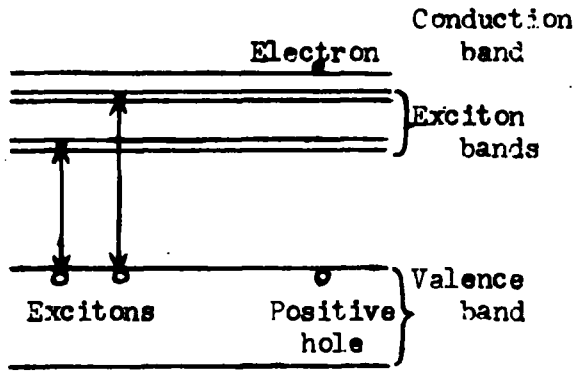


Fig. 5. Energy bands in ionic solids.

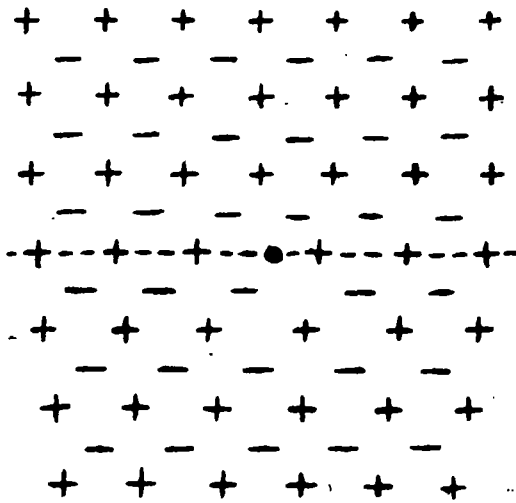


Fig. 7. Edge dislocation in an alkali halide.

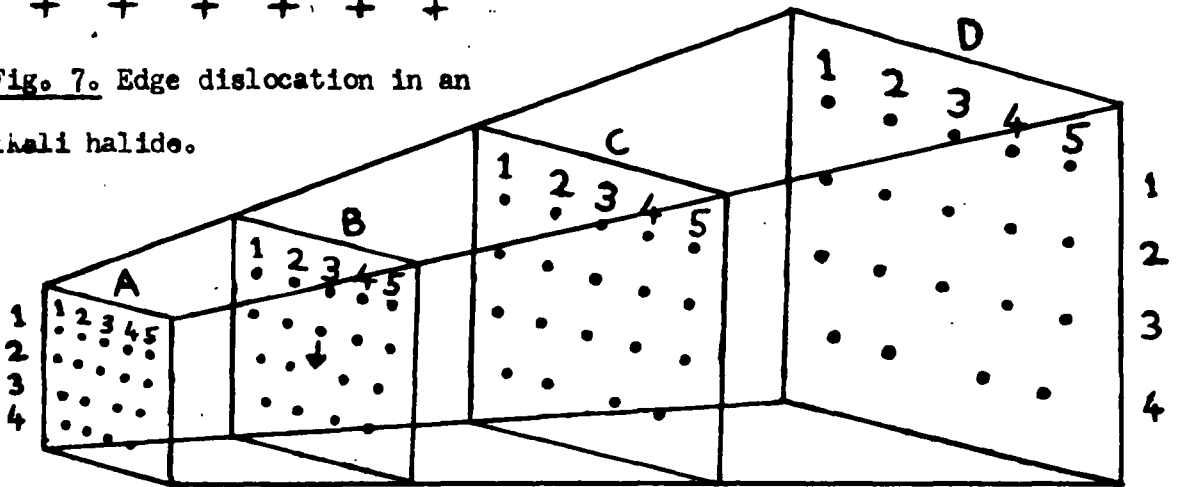


Fig. 8. Production of vacancies from an edge dislocation.

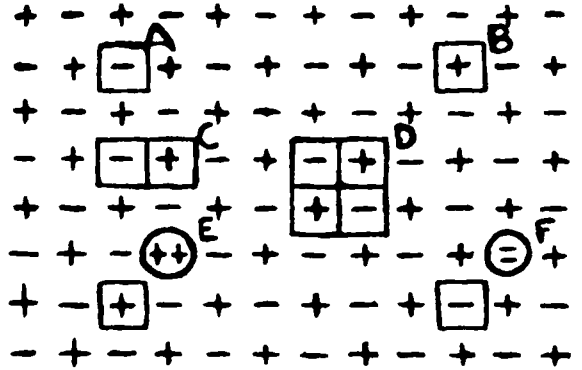


Fig. 6. Possible vacancies and vacancy aggregates in alkali halides.

ions would be less than 1% of the number of vacancies on the basis of these calculations. Frenkel effects predominate, however, in the silver halides where the ionic radii are much more unequal.

Possible combinations of vacant lattice sites in the alkali halides are shown in figure 6. A and B represent a cation and an anion vacancy, with a negative and positive charge respectively. C represents a vacancy pair formed by combination of A and B with neutralisation of charge; D depicts a quartet. Impurity multivalent ions present in the lattice will have vacancies associated with them, E and F, for reasons of electrical neutrality which will tend to be in nearest neighbour positions on account of the electrostatic attraction. It was originally thought that lattice vacancies were formed on the surface of the crystal or on the surfaces of internal cracks, and then diffused into the bulk. Obviously, equal numbers of cation and anion vacancies must diffuse at the same rate, otherwise portions of the crystal will become charged; this suggests that pairs of vacancies are responsible, as does the fact that the jump frequency of anion vacancies is very low-Seitz (15).

Recently, mechanisms for the formation of vacancies from crystal dislocations have been proposed. A simple such dislocation is the Taylor-Crowan or edge dislocation, which can be formed, in the alkali halides, by the insertion of two partial extra planes of ions. Figure 7 shows such a dislocation; the plane of the paper represents a (001) face of the crystal. The dislocation line is perpendicular and passes through the black dot indicated; the dashed line represents the (110) plane at which the extra (110) planes terminate, and is called a slip plane. Motion of the dislocation line is restricted mainly to the slip plane; if two such dislocations of opposite orientation, whose slip planes are separated by a few ionic spacings should chance to coincide, then a series of vacancies will be formed between the slip planes.

A more sophisticated mechanism proposed by Seitz (29) requires an irregular edge to the extra planes. Schematically this is shown in figure 8 where the extra

plane of atoms all numbered 3 extends across all the planes in rows 1 and 2 but only across planes C and D in row 3. If atom 3 row 2 plane B drops down to row 3 in the same plane, the partial plane of atoms is extended by one unit, and a vacancy is formed which can diffuse away. Such a mechanism is an excellent explanation for the formation and destruction of vacancies, and indicates that dislocations can act as a source and sink for them.

### 3. Colour centres in alkali halides

Alkali halide crystals absorb electromagnetic radiation in the far infra red due to ionic vibrations and also in parts of the ultraviolet, where excitons and conduction band electrons are generated optically. Elsewhere, they are quite transparent in the absence of coloured impurities. On X-irradiation, however, characteristic colours, varying with the temperature are produced; thus at room temperature NaCl becomes brown and KCl magenta. The colours are ascribed by Seitz (16) to various "colour centres" considered below, and drawn in figure 9.

(i) The F centre: ("Farbenzentren" i.e. colour centres) is characterised by a prominent band (called the F band) peaking generally in the visible; at  $5630\text{\AA}$  for KCl, for example. It is considered to be a single electron trapped at an anion vacancy and can be produced either by high energy radiations, or by heating the alkali halide in alkali metal vapour. In the former, a conduction band electron or exciton can interact with either an isolated anion vacancy or a pair, in which case the cation vacancy diffuses away as does the hole associated with the exciton. On heating in alkali metal vapour, some alkali metal is adsorbed on the surface of the crystal where it ionises, the electron going into the conduction band from which it produces F centres as before (3). Good evidence for the correctness of the F centre model is obtained from the fact that the F band is independent of the nature of added alkali metal; also Witt (31) has shown that the observed decrease in density is, within experimental error, compatible with the formation of a single anion vacancy for each F centre formed.

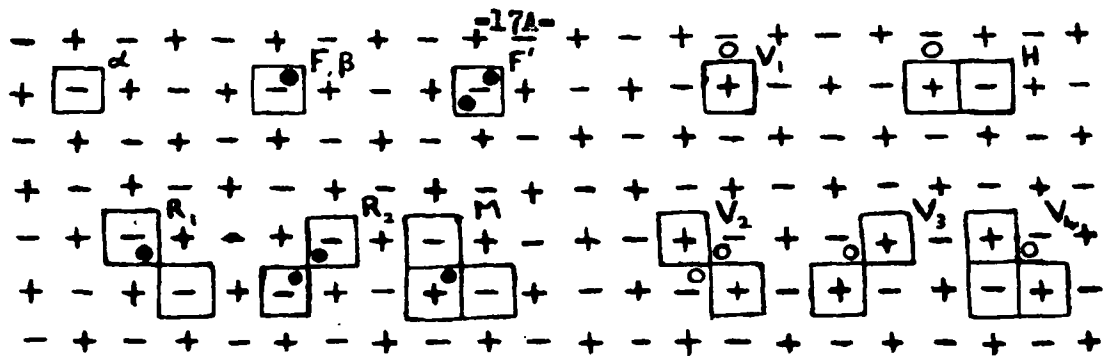


Fig. 9. Colour centres in alkali halides; Seitz (16).

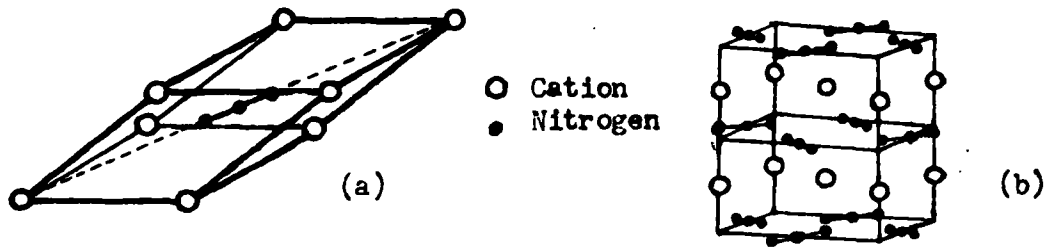


Fig. 10. Crystal structures of (a)  $\text{NaN}_3$  and (b)  $\text{KN}_3$ .

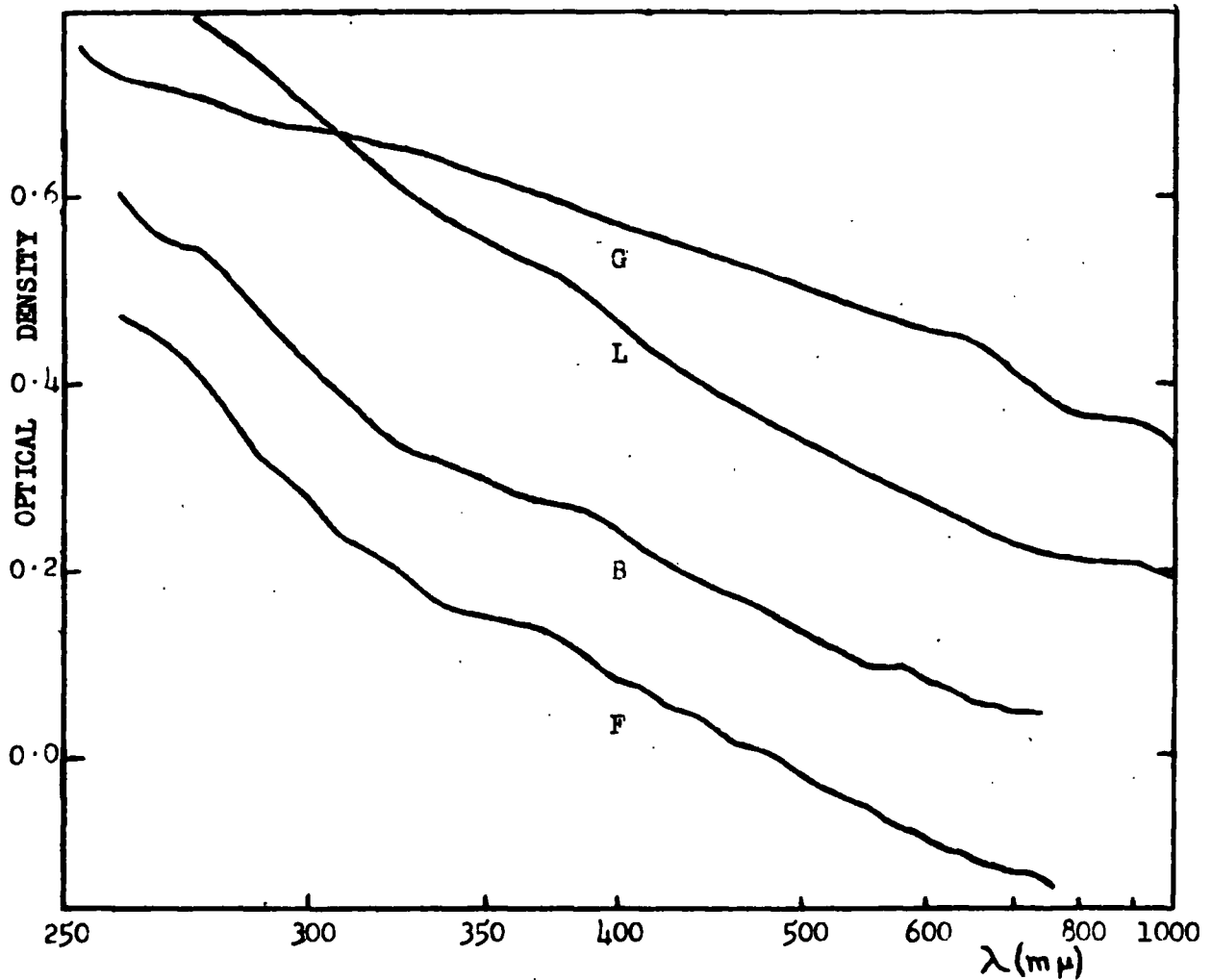


Fig. 11. Four spectra of unirradiated  $\text{NaN}_3$ .

The F band is a good bell shaped band, which becomes very narrow at low temperatures, showing that the single transition involved is between two discrete energy states. In some crystals (KCl) a small shoulder and tail has been observed on the high energy side of the band; Duerig and Markham (32) have shown that this shoulder bears a constant ratio of 0.047 to the height of the F band. Seitz (16) calls it the K band, and Mott and Gurney (33) consider it is due to a transition to a higher state, while the tail is due to a transition to the ionisation continuum. They add that it is not clear why the continuous absorption should be so much weaker than the band absorption.

F centres can be bleached by irradiating with light lying in the F band, when such crystals become photoconducting; the incident light is only sufficient to raise the F electron to an excited state, from which it is thermally ionised to the conduction band even at temperatures of the order of  $-200^{\circ}\text{C}$ .

(ii) F<sup>+</sup> centre. When an alkali halide crystal containing F centres is irradiated with F light at fairly low temperatures, below  $25^{\circ}\text{C}$  for NaCl and  $-75^{\circ}\text{C}$  for KCl, the F band diminishes and a new band, called the F<sup>+</sup> band by Pohl appears on the long wavelength side; for KCl it peaks about  $7300\text{\AA}$ . Pick (34) measured the quantum efficiency with which F centres are destroyed in the formation of F<sup>+</sup> centres and found it is close to 2 in KCl for temperature around  $-100^{\circ}\text{C}$ ; to explain this, he proposed that the F centre electron is raised to the conduction band with a little thermal help, and is then trapped by another F centre. Two F centres are then destroyed per incident quantum absorbed; the entity produced, with two electrons trapped at an anion vacancy, is the F<sup>+</sup> centre and confers a local negative charge on the lattice.

The F<sup>+</sup> band is invariably much broader than the F band and overlaps with it; its width is relatively insensitive to temperature, suggesting that the transition is to a continuum. Seitz (15) notes that this is in qualitative agreement with the behavior of such single charged negative ions as  $\text{H}^-$ . F<sup>+</sup> centres can be bleached to F centres by F<sup>+</sup> light, and also by heat.

(iii) R<sub>1</sub>, R<sub>2</sub>, M and N bands All these bands are obtained on irradiating crystals containing F centres with F light at temperatures above those at which F' centres are stable. Not much is known about any of them; models proposed by Seitz are given in figure 9 for the first three. M centres are bleached by M light, and the crystal becomes photoconducting; but both R centres are stable to R light. Seitz (15) proposes that such centres are analogues of diatomic molecules, and that in the excited state the vacancies separate somewhat so that the first electronic excited state gets much closer to the ground state. The system then makes an almost adiabatic transition and returns to the ground state. All these bands occur on the long wavelength side of the F bands; for KCl at room temperature the values are about 6700Å° and 7300Å° for the R bands, 8200Å° for the M band, and 9700Å° for the N band.

(iv) Colloid bands. When crystals containing F centres are heated to high temperatures, sometimes with irradiation by F light as well, further bands are obtained on the long wavelength side of the F band which are ascribed to the presence of colloidal metal. By irradiating F centred KCl with F light at 100°C, Scott and coworkers (35) obtained a broad highly composite band called the R' band, which is probably a combination of the R, M, N bands together with other aggregates. By heating alone to 300°C, gives a relatively narrow pure colloid band which peaks at 7750Å° for KCl, and which grows at the expense of the F band. Savostianova (36) has applied the Mie(37) theory of the scattering of light by metallic spheres to particles of alkali metal embedded in alkali halides, and obtained bands of similar shape; on the basis that the diameter of the colloids is small compared to the wavelength of the incident light, it can be calculated for K in KCl that the colloid band should peak at 7300Å°, in fair agreement with experiment.

(v) V bands are produced by irradiation at low temperatures simultaneously with F centres or by addition of excess halogen on heating in halogen vapour,

without F centres; they are ascribed to the interaction of holes with lattice vacancies. The V system is much less certain than the F band system; current assignments are indicated in figure 9. Best characterised is the  $V_1$  band, produced in KCl (38) by X-irradiation at low temperatures; it vanishes above  $-100^\circ\text{C}$  and peaks at  $3600\text{\AA}$ . The  $V_1$  centre responsible is regarded as the anti-morph of an F centre; that is, as a hole trapped at a cation vacancy, and Kanzig (39) has shown by electron spin resonance techniques that the hole is localized on two of the halide ions surrounding the vacancy. The  $V_2$ ,  $V_3$  and  $V_4$  centres are regarded as the antimorphs of the  $R_2$ ,  $R_1$ , and M centres respectively; all are more stable than the  $V_1$  centre, the  $V_2$  and  $V_3$  centres being stable at room temperature. In KCl the bands peak at  $2300\text{\AA}$  for  $V_2$ ,  $2150\text{\AA}$  for  $V_3$  and  $2540\text{\AA}$  for  $V_4$ . The diatomic nature of the  $V_2$  and  $V_3$  centres was recognised by their discoverer Mollwo, who, using additively coloured crystals, noted that their concentration varied with the first power of the pressure of the diatomic halogen vapour; similarly, the concentration of F centres varied with the first power of the monatomic alkali metal vapour. The  $V_3$  has a net negative charge which should make it resistant to bleaching by electrons; Casler, Pringsheim and Yuster (38) have found that photoelectrons from F centres at room temperatures bleach  $V_2$  centres with high efficiency, but hardly affect  $V_3$  centres at all. Evidence has also been obtained by Dutton and Maurer (40) that  $V_1$  centres bleach by evaporation of the hole which is either annihilated at an F type centre, or trapped by a  $V_3$  centre to give a  $V_2$ .

(vi) Miscellaneous bands. Various other bands have been obtained in the alkali halides by suitable treatment. Impurity bands due to  $\text{H}^-$  addition, called U bands, and divalent alkaline earth ions, called Z bands, have been described. The H band, formed by irradiation at very low temperatures, is very similar to, and peaks a little on the ultraviolet side of the  $V_1$  band; Seitz (16) ascribes it

to a hole trapped at a vacancy pair. The  $\alpha$  and  $\beta$  bands peak a little to the long wavelength side of the first fundamental absorption band, the  $\alpha$  being the longer; Seitz ascribes them to electronic excitations of the halide ions to levels not found in the perfect crystal. The close correlation in intensity between the F and  $\beta$  bands indicates that the latter is associated with a halide ion adjacent to an F centre, while the  $\alpha$  band is that adjacent to an anion vacancy.

#### 4. Crystal Structures

The alkali metal halides crystallise in the face centred cubic form with the exception of CsCl, CsBr and CsI, which are body centred cubic. The azides, however, containing the linear  $N_3^-$  ion, have considerably lower symmetry;  $NaN_3$  crystallising in the trigonal form (41) with the azide ions all parallel.

Figure 10a, while  $KN_3$ ,  $RbN_3$  and  $CsN_3$  crystallise in a body centred tetragonal mode (42) with successive azide ions at right angles to each other, Figure 10b.

The crystallographic measurements of the unimolecular unit cell of trigonal  $NaN_3$  are  $a = 5.488 \text{ \AA}$ ,  $\alpha = 38^\circ 43'$ ; for tetragonal  $KN_3$ ,  $RbN_3$ ,  $CsN_3$ ,  $a = 6.094, 6.36, 6.72 \text{ \AA}$  and  $c = 7.057, 7.41, 8.04 \text{ \AA}$  respectively, with four molecules to the unit cell. The N-N distances are equal at  $1.16 \pm 0.02 \text{ \AA}$  for all the azides quoted.

### Results

#### 1. Processing of spectra

The spectra figured in this work were calculated as the difference of two experimental records, which were obtained on a linear wavelength scale; the results have been converted to a scale linear in energy. For unirradiated crystals the spectrum of the quartz windows with the crystal holder in position was subtracted from that obtained with the crystal in place; the latter in turn, was subtracted from the irradiated crystal record to give the spectrum due to the irradiation. Measurements had to be made under the same temperature conditions as there was a considerable contraction of the inner part of the metal dewar on cooling to liquid nitrogen temperatures, and also because the spectrum of the unirradiated

crystals varied with temperature. Figure 11 shows four spectra of unirradiated  $\text{NaN}_3$  taken at liquid nitrogen temperature, in which for E and F the quartz window spectra were taken at room temperature. Unless otherwise stated, all measurements were taken at liquid nitrogen temperatures to get the best resolution.

The reproducibility of the experimental records was, for the "UV" and "VIS" regions, about that stated by the makers, namely  $\pm 0.002$  absorption units at optical density 1.0 and  $\pm 0.005$  near 2.0. In the "IR", however, there were sometimes discontinuous jumps occurring between successive I.R. spectra; these discontinuities may be due to changes in the "IR" lamp filament resulting when the lamp is switched on and off. Discrepancies between the regions have been removed in the spectra figured by matching the absorptions with the "VIS" region, which was taken as the standard since the alignment of the crystals was checked in that region.

The temperature of the crystal was checked with a thermocouple soldered to the bottom of the crystal holder; it was found impracticable to have the thermocouple directly in contact with the crystal. At liquid nitrogen temperatures,  $-196^\circ\text{C}$ , the reading was  $-180 \pm 5^\circ\text{C}$ . Room temperature refers to temperatures about  $20^\circ\text{C}$  stabilised by means of an acetone bath in the dewar.

## 2. Spectra of unirradiated azides

### (i) Spectra below absorption edge

(a) Variation in Spectra. Figure 11 gives the spectra of four crystals of  $\text{NaN}_3$  at liquid nitrogen temperatures, showing some variation in slope; this can be accounted for by noting that the crystals did not have plane surfaces and were probably not set at right angles to the spectrophotometer beam. The fine structure noticeable in B and F may be due to impurities since these crystals came from a different recrystallisation to G and L.

(b) Comparison of spectra. The spectra of the four azides is given in figure 12.

The magnitudes of the absorption are not strictly comparable since the crystals varied in thickness from about 0.1 mm. for  $\text{NaN}_3$  and  $\text{CsN}_3$  to 0.3 mm. for  $\text{KN}_3$  and  $\text{RbN}_3$ ; also different hole apertures were used, 3 mm. square for  $\text{NaN}_3$  and  $\text{RbN}_3$ , 4 mm. square for  $\text{KN}_3$  and  $\text{CsN}_3$ . Nevertheless, it can be seen that the better crystals of  $\text{RbN}_3$  and  $\text{CsN}_3$  attenuate the light beam less than the other two azides. The explanation of the slopes of the spectra and their decrease from  $\text{NaN}_3$  to  $\text{CsN}_3$  is uncertain. Similar slopes have been observed in Ag, Tl and Cd halides, where they have been explained (43) on the basis of impurity atoms, atoms in unusual position, or forbidden transitions; the latter has been used to account for their absence in alkali halides. Isetti and Neubert (44) working with NaCN have explained their slopes on the basis of Debye and Bueche's (45) calculations on the scattering of light by inhomogeneous solids.

(ii) Spectra at absorption edge

(a) Experimental. The spectra of the absorption edges, suitably shifted for clarity, are shown in figure 13a. The absorption edge energy generally decreases for larger cations; a result at variance with that obtained by Jacobs and Tompkins (9) quoting reflectance spectra of  $\text{NaN}_3$ ,  $\text{KN}_3$  and  $\text{BaN}_3$  shown in figure 13b.

(b) Interpretation. By analogy with the alkali halides the absorption can be attributed to the low energy tail of an exciton band, whose peak can be very approximately calculated by the method of von Hippel (43) (44).

The formula for the energy of the exciton transition is:

$$h\nu_{\text{calc}} = W - W_p - \Omega_+ - \Omega_-$$

Here  $W$  is the work done in transferring an electron from an anion to a neighbouring cation, and is calculated from a cycle, giving the following formula:

$$W = \frac{(2\alpha - 1) e^2}{\gamma_0} + E - I$$

where  $\gamma_0$  is the smallest interionic distance in the crystal and

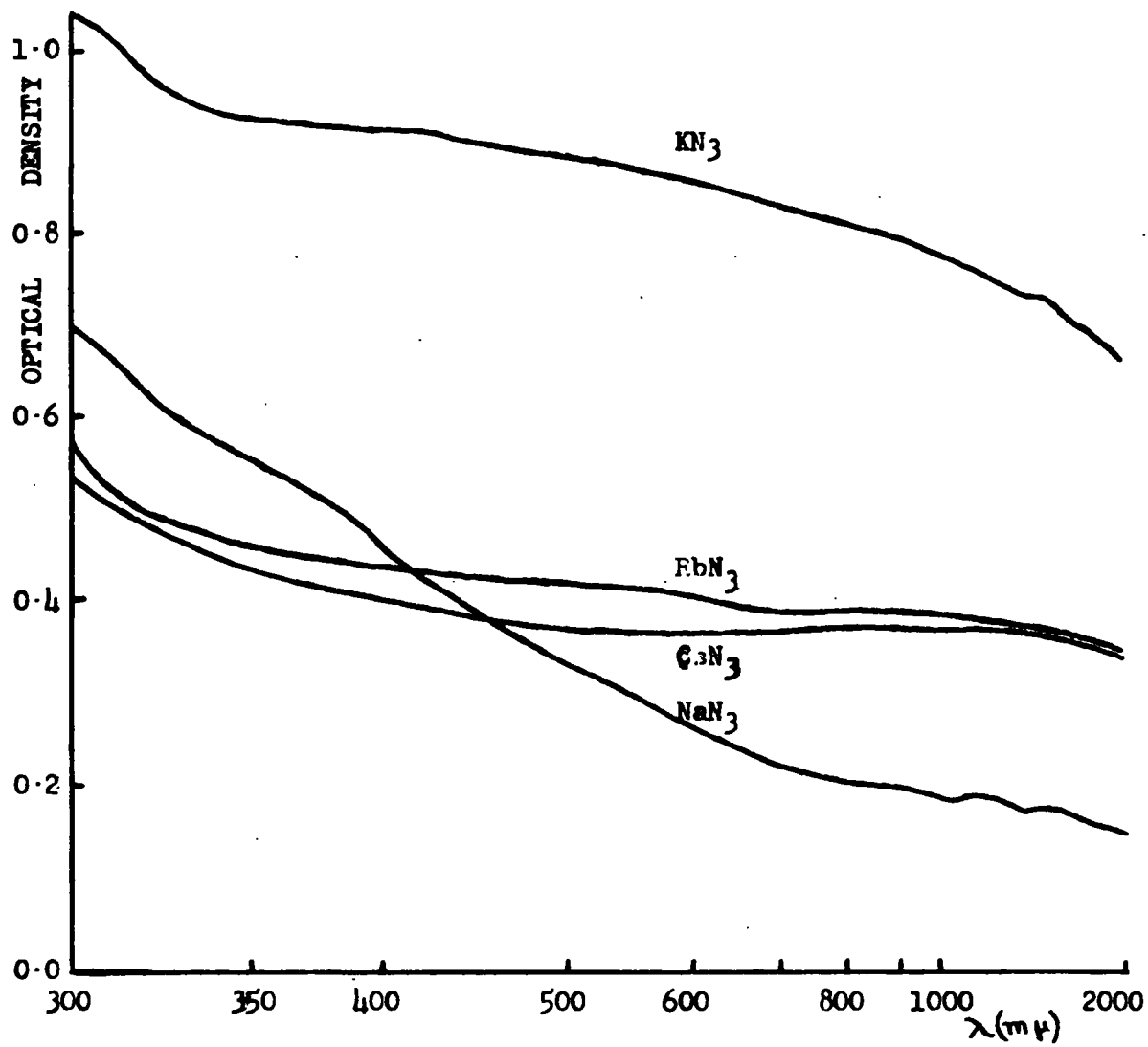


Fig. 12. Unirradiated azide spectra below absorption edge.

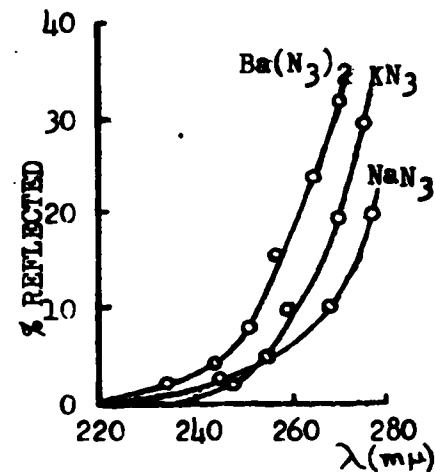


Fig. 13(b). Absorption edges (9).

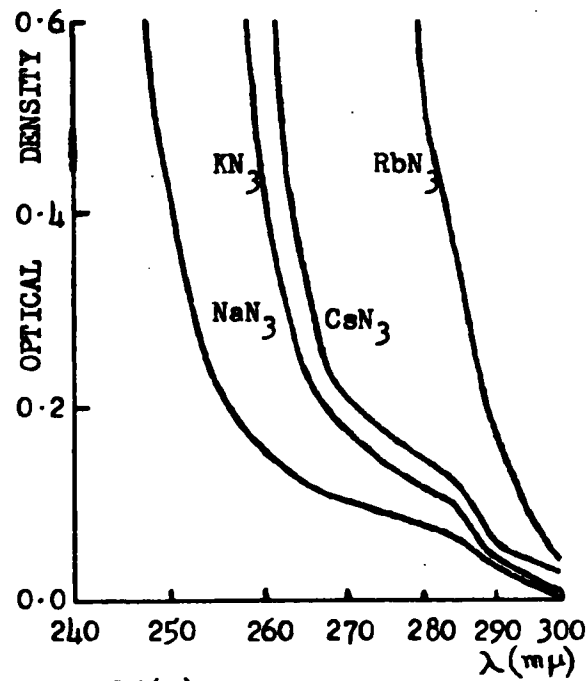


Fig. 13(a). Absorption edges.

Table II. Calculations on Exciton Absorption Bands.

All energies in electron volts

<u>Salts</u>	W	$W_p$	$\Omega_+$	$\Omega_-$	$h\nu_{calc.}$	$h\nu_{obs.}$
NaBr	10.4	1.7	1.7	0.3	6.7	6.50
KBr	10.1	1.4	1.6	0.2	6.9	6.58
RbBr	9.8	1.4	1.5	0.2	6.7	6.43
NaN <sub>3</sub>	7.0	1.2	1.7	0.3	3.8	
KN <sub>3</sub>	9.6	1.1	1.6	0.2	6.7	
RBN <sub>3</sub>	8.9	1.0	1.5	0.2	6.2	
CsN <sub>3</sub>	8.7	1.0	1.4	0.2	6.1	

was calculated from the crystallographic data.

$\alpha$  is the Madelung constant referred to  $r_0$ ; for  $\text{NaN}_3$ , a value due to Højendahl (48) was used, while for the others it was calculated from the Madelung energies quoted by Gray and Waddington (49) to whom is also due a value for

E the electron affinity of the azide radical.

I represents the ionisation potential of the cation; values are taken from Evans and Yoffé (42)

$W_p$  of the first equation, represents the polarisation energy change and is given by a formula due to Klemm (50)

$$W_p = \frac{2.027 e^2}{r_0^4} (\alpha_1 + \alpha_2)$$

where  $\alpha_1$  and  $\alpha_2$  are the polarisabilities of the anion and cations. For the cations, the data of Tessman, Kahn and Shockley (51) have been used, and a value, 4.4, for the azide anion has been obtained from the formula quoted therein:

$$\alpha_{\text{N}_3^-} = \frac{3 V_m}{4 \pi} \frac{N^2 - 1}{N^2 + 2} - \alpha_{\text{K}^+}$$

where  $V_m$  is the crystallographic volume ( $\text{Å}^3$ ) per molecule of  $\text{KN}_3$  and  $N$  is the refractive index, given as 1.66 by Dreyfus and Levy (52).

$\Omega_+$  and  $\Omega_-$  are the interaction energies of the neutral atoms, formed as a result of the electron transfer with neighbouring ions and values quoted (47) for the corresponding bromides have been used.

The results are shown in Table II, together with some data for the corresponding bromides for comparison. It should be pointed out that while these calculations can fairly accurately be applied to the alkali halides, where the error is usually less than 0.4 electron volts, Mott

and Gurney (53) express doubts whether they would hold for other polar crystals. The value calculated for  $\text{NaN}_3$  is obviously in error, since from the experimental data it must be greater than 5 eV; but the value for  $\text{KN}_3$  may well be fairly accurate, since for the similar  $\text{KCNS}$  the experimental value is 6.7 electron volts (54). The calculations do indicate however that the absorption edge energy should decrease for larger cations.

### 3. Spectra of azides irradiated at liquid nitrogen temperatures

When the alkali metal azides were irradiated at liquid nitrogen and room temperatures, two very different series of spectra were obtained, as can be seen by comparison of Figures 14-17, 18, and Figures 19-21. The series were related since on warming samples irradiated at liquid nitrogen temperature to room temperature, the room temperature spectra resulted. As the low temperature spectra are the more explicable in terms of the alkali halide models, they are considered first. Inspection of the figures 14-17, 18 shows that these spectra have broadly similar features; a prominent single band near 600  $\mu$ , hereinafter referred to as the "A" band, a prominent (except in  $\text{NaN}_3$ ) multiple band peaking near 380  $\mu$ , the "B" band, and a weak band beyond 700  $\mu$  which will be called the "C" band.

(i) "A" band. The measurements of this band are given in table 3, along with data for certain alkali halide "F" bands measured at similar temperatures; the correspondence between the two bands obviously suggests that the "A" band is the F band of the alkali metal azides. Note in particular that  $\lambda_{\text{max}}$  at 612  $\mu$  for the six coordinate  $\text{NaN}_3$  with the internuclear distance  $3.26\text{\AA}$  is almost identical with the  $\lambda_{\text{max}}$  at 609  $\mu$  and 605  $\mu$  for six coordinate  $\text{KBr}$  and  $\text{RbCl}$ , both with internuclear distance  $3.29\text{\AA}$ .

In order to explain some other features of the A band the nature of the F centre, an electron trapped at a vacant anion site, must be considered further, several theoretical studies on such systems are quoted by Seitz (16). Absorption

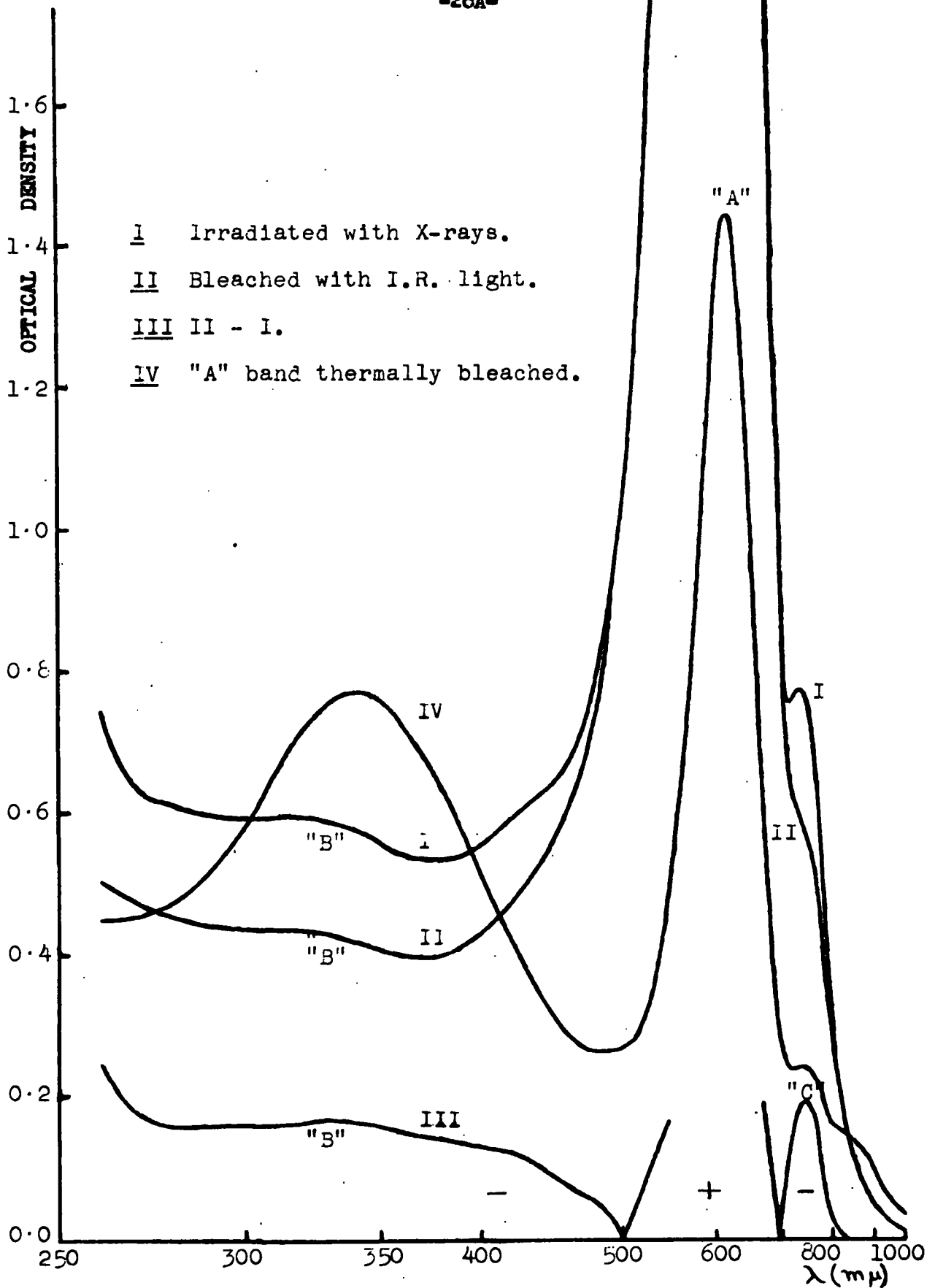


Fig. 14.  $\text{NaNO}_3$  irradiated at liquid nitrogen temperature.

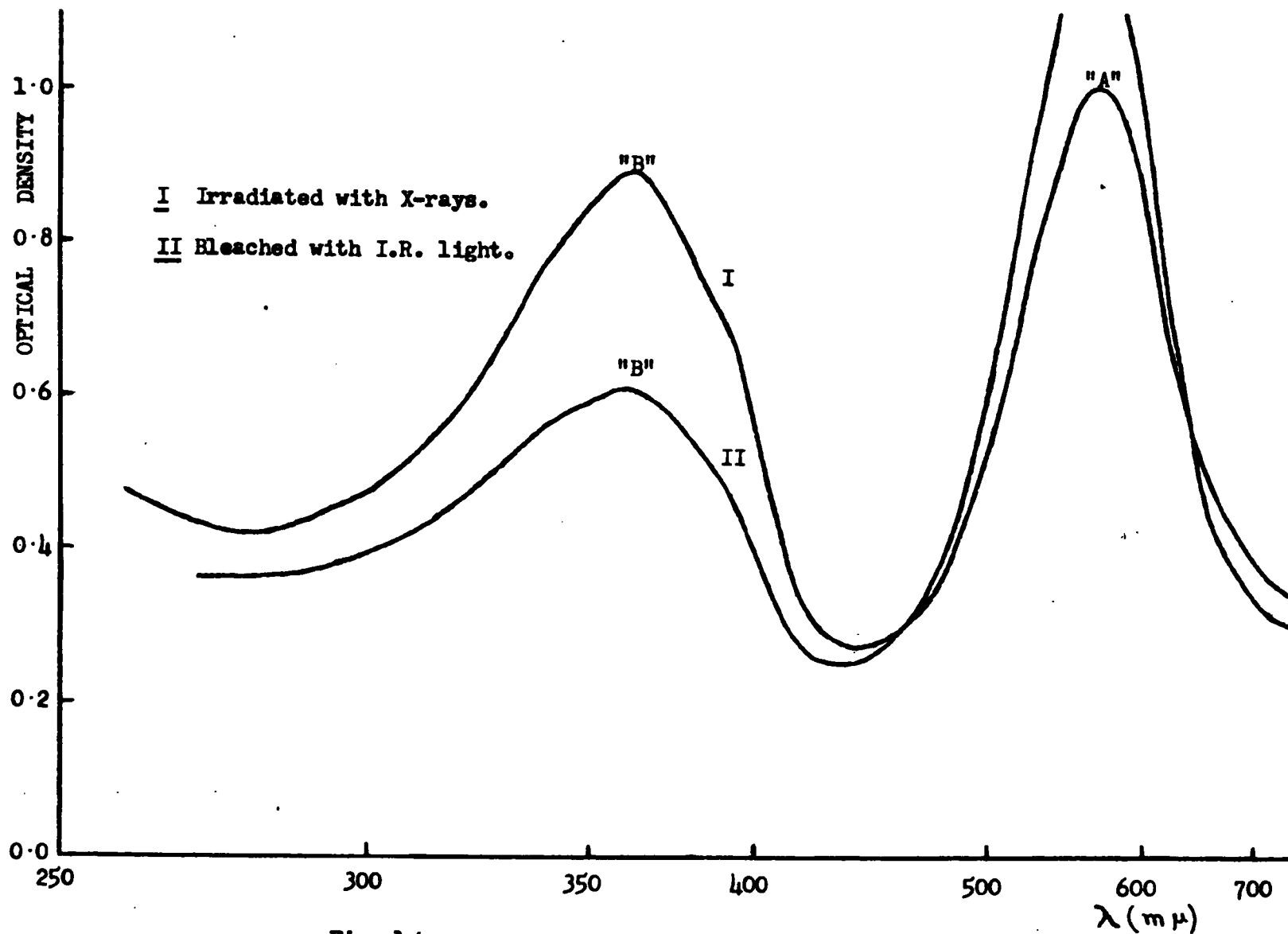


Fig. 15.  $KN_3$  irradiated at liquid nitrogen temperature.

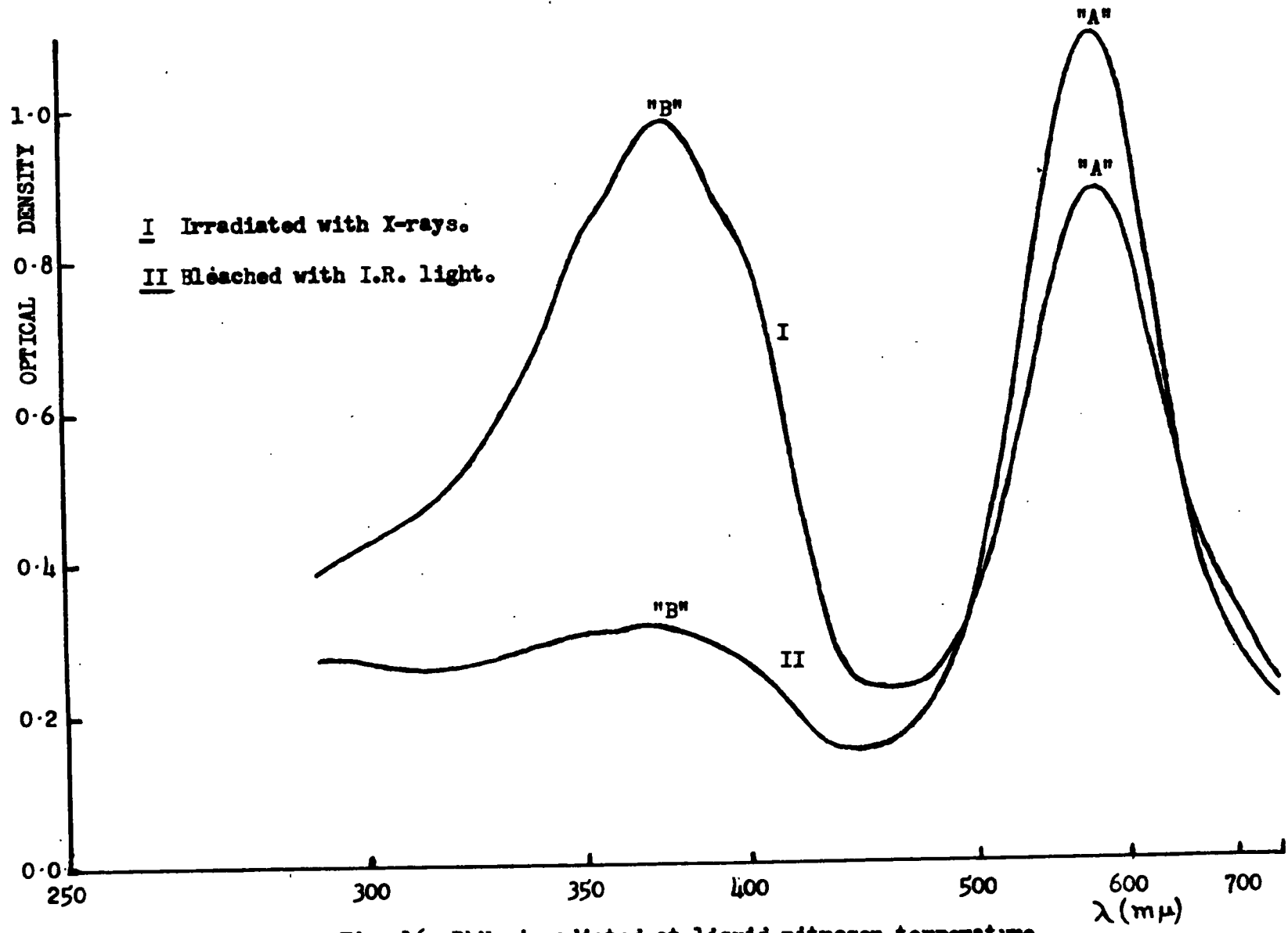


Fig. 16.  $RbN_3$  irradiated at liquid nitrogen temperature.

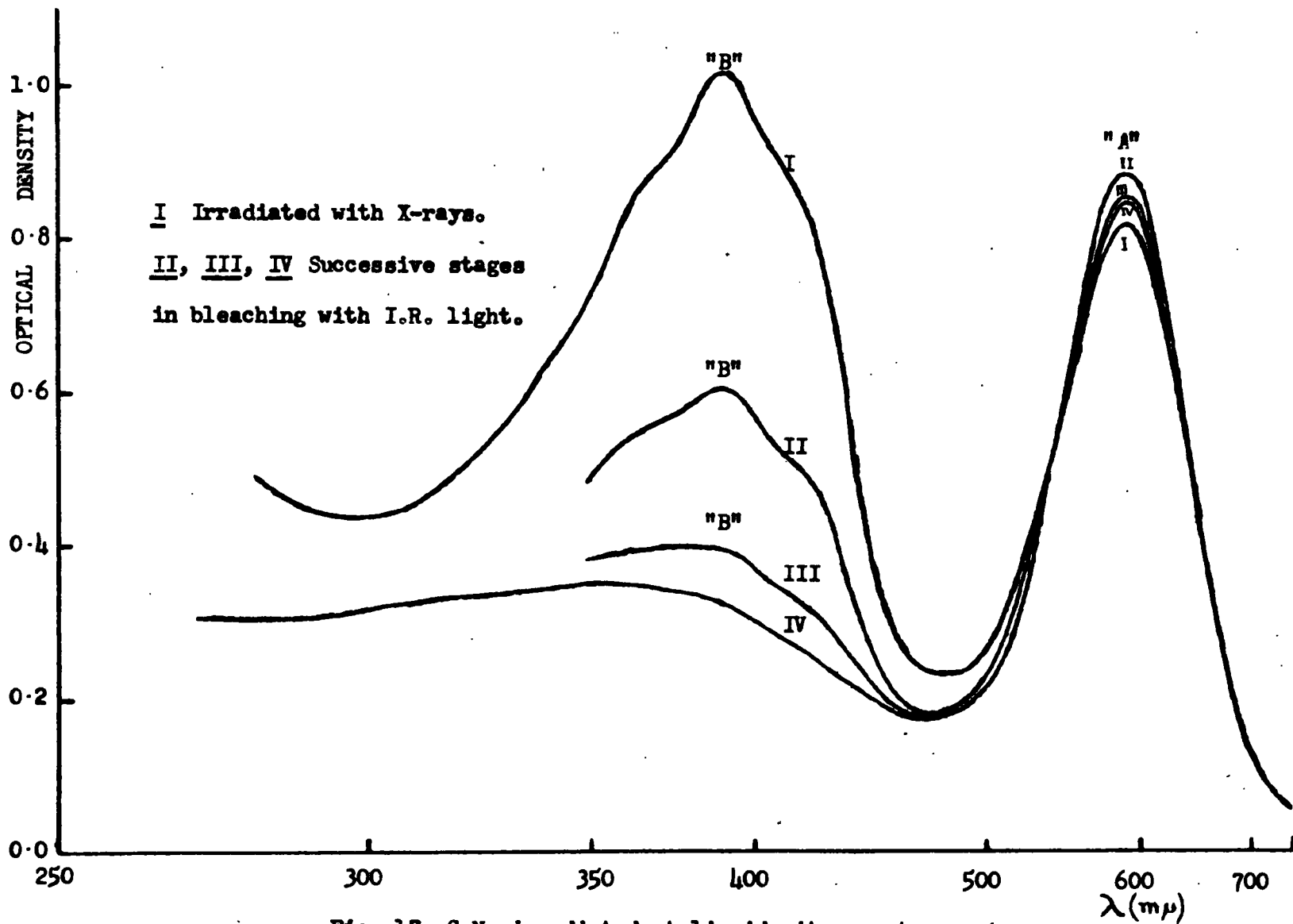


Fig. 17.  $\text{CsN}_3$  irradiated at liquid nitrogen temperature.

Table III. Comparison of alkali metal azide A band with alkali halide F band (54)  
at  $\sim -180^\circ \text{C}$ .

<u>Salt</u>	Interionic distance $r_0$ ( $\text{\AA}$ )	$\lambda_{\text{max}}$ ( $\mu$ )	$E_{\text{max}}$ (eV)	bandwidth (eV)
		<u>A Band</u>		
$\text{NaN}_3$	3.26	612	2.03	0.32
$\text{KN}_3$	3.52	568	2.18	0.60
$\text{RbN}_3$	3.68	578	2.14	0.50
$\text{CsN}_3$	3.92	592	2.09	0.43
		<u>F Band</u>		
$\text{NaCl}$	2.81	455	2.72	0.34
$\text{KCl}$	3.14	548	2.26	0.23
$\text{KBr}$	3.29	609	2.04	0.22
$\text{RbCl}$	3.29	605	2.05	0.22
$\text{RbBr}$	3.43	665	1.86	0.19

of light by an F centre results in excitation of the electron from an s to a p state, the energy of the transition being modified by the interaction of the electron with the surrounding ions. This interaction raises the s and p energy levels and separates them further; as the p state with its larger radius interacts more strongly than the s state; the interaction energy depends on the distance and number of the surrounding ions, but only slightly on their nature (in the alkali halides).

Now  $\text{KN}_3$ ,  $\text{RbN}_3$  and  $\text{CsN}_3$  all have the same body-centred tetragonal crystal lattice in which the interionic distance ( $r_0$ ) increases in the order given. For an F centre in such a lattice, the interaction energy would be greatest for  $\text{KN}_3$  and least for  $\text{CsN}_3$ ; it is therefore expected that the energy of the corresponding F band would decrease in the same order, as found experimentally for the A band. Following Ivey (55) an empirical formula can be deduced relating the interionic distance  $r_0$  with  $\lambda_{\text{max}}$  of the form  $\lambda_{\text{max}} = A r_0^n$ , where A and n are constants; plotting  $\log r_0$  against  $\log \lambda_{\text{max}}$  gives three points lying almost perfectly on a straight line, and the formula:

$$\lambda_{\text{max}} = 3520 r_0^{0.38} \quad (\text{A}^\circ)$$

with mean error less than  $10\text{A}^\circ$ . For comparison, Ivey quotes:

$$\lambda_{\text{max}} = 703 r_0^{1.84} \quad (\text{A}^\circ) \quad \text{for the alkali halide F band at room}$$

temperature, with mean error of  $130\text{A}^\circ$ ; the higher power reflects the much greater dispersion of the F band. Applying Ivey's formula to the six coordinate trigonal  $\text{NaN}_3$  with  $r_0 = 3.26\text{A}^\circ$ ,  $\lambda_{\text{max}} = 6185\text{A}^\circ$ , which would move to shorter wavelengths at lower temperatures, the observed value of 612 mu at liquid nitrogen temperatures is therefore in fair agreement. Noteworthy is the fact that Ivey's formula does not work well for  $\text{KBr}$  and  $\text{RbCl}$  with  $r_0 = 3.29\text{A}^\circ$ , which gives  $\lambda_{\text{max}} = 629$  mu; the observed values are 652 and 647 mu respectively.

So far only the interaction of the F electron with neighbouring ions in their mean positions has been considered. Such ions, however, oscillates in tune with the lattice vibrations or phonons, and therefore their interactions with the F electron will vary in time. Since the time required for an electronic transition is much shorter than that required for one ionic vibration (the Franck-Condon principle), the interaction effect on the observed transition will depend on the instantaneous positions of the surrounding ions and not on their mean position. For this reason, the transition is observed not as a single line, but as a band with the form of the Gaussian error curve; becoming narrower at low temperatures where the lattice vibrations are weaker. As a measure of the broadening the band width at half height is quoted in table III. Comparisons of the bandwidths of KBr and RbCl (both 0.22eV) with  $\text{NaN}_3$  (0.32 eV), all three salts having approximately the same interionic distance, and the same sixfold coordination number, shows that the latter has a significantly greater bandwidth, which may be due to interactions with the vibrations of the nearest azide ions. The much larger bandwidths of  $\text{KN}_3$ ,  $\text{RbN}_3$  and  $\text{CsN}_3$  can be ascribed (12) to interactions with a larger number of ionic oscillators not only with the eight nearest cations, but also with two longitudinal  $\text{N}_3^-$  ions.

Another feature of these bands is their markedly skew character as shown by the flatter slopes on the high energy sides. The extent of this skewness can be roughly measured by comparing the bandwidths on either side of  $\lambda_{\text{max}}$ , the ratio high energy: low energy bandwidth is about 1.2 for all the azides. The skewness cannot be due to the sluggish response of the Cary recorder, since scanning in either direction gave the same curve; nor can it be due to overlap of the B band, since this does not occur strongly in  $\text{NaN}_3$ .

Tompkins and Young (12) irradiated potassium azide at liquid nitrogen temperatures with U.V. light and obtained a band similar to the A band : peaking at 550 mu, which they ascribe to F centres. They add: 'Limited F-centre

formation can also occur at vacant anion sites within the stress fields of edge dislocations, and these F-centres may absorb at liquid nitrogen temperatures at wavelengths slightly different from 550  $\mu$ . The initial formation of a small concentration of centres which absorb at 535  $\mu$  is ascribed to such an effect. The centres are formed first because excitons migrate preferentially towards dislocations, and they are formed in limited extent because vacant anion sites cannot migrate towards dislocations under the conditions of irradiation.'

A continuous series of such centres in slightly different environments could account for the flatter slope on the high energy side of the A band. The absorption coefficient for UV light is much greater than that for X-rays, and hence radiation damage near the surface of the crystal will be relatively more important for the former. A large surface component might possibly account for the discrepancy between the 550  $\mu$  of Tompkins and the 568<sup>#</sup> 2  $\mu$  of the present work.

(ii) B band. The data for this band is summarised in table IV, from which an Ivey (55) formula can be calculated for the principal peak in the higher azides:

$$\lambda_{\max} = 1470 r_0^{.716} (\text{\AA}^\circ)$$

with maximum error 10 $\text{\AA}^\circ$ . The agreement between formula and experiment: not quite as good as that for the A band.

The most noticeable feature of this band is its similarity in all three of the higher azides. There is a steep low energy and flatter high energy slope; the shoulders on each side occur at about the same (equal) energy difference from the principal peak, and the total bandwidth is about 1 eV. The only differences are the shift of the whole band to longer wavelengths from  $\text{KN}_3$  to  $\text{CsN}_3$  and the corresponding increasing distinctness of the shoulders. The close association of the shoulders and peak is

Table IV. Comparison of the alkali metal azide B band with the alkali halide  $V_1$  band (54) at  $-180^\circ\text{C}$ .

<u>Salt</u>	<u>B Band</u>			
		High energy shoulder	Peak	Low energy shoulder
$\text{KN}_3$	$\lambda$ ( $\mu$ )	340	361	390
	E (eV)	3.65	3.43	3.18
$\text{RbN}_3$	$\lambda$	350	374	400
	E	3.54	3.31	3.10
$\text{CsN}_3$	$\lambda$	365	390	420
	E	3.40	3.18	2.95
$\text{NaN}_3$	$\lambda$		330	
	E		3.76	

Salt:	<u><math>V_1</math> Band</u>							
	KCl	RbCl	KBr	RbBr	mixed crystals			
$\lambda$ ( $\mu$ )	356	359	410	420	3KCl:RbCl	3KCl:2KBr	359	385
E (eV)	3.48	3.45	3.02	2.95	3KCl:RbCl	3KCl:2KBr	3.45	3.22

suggested by the similar behavior on bleaching with I.R. light, figure 17, and all three peaks may therefore be due to the same centre. The strong similarities between the higher azides indicate that such a centre is probably more closely connected with the common azide anion than with the cations, and therefore is a V type centre involving trapped positive holes.

The most probably alkali halide model responsible for the B band is the  $V_1$  centre, since its band is the only one occurring in the same spectral region; at 356  $\mu$  in KCl and 410  $\mu$  in KBr, for example. The other V bands are much further in the ultraviolet, just on the long wavelength side of the first fundamental band; the longest,  $V_4$ , occurs at 254  $\mu$  in KCl and 275  $\mu$  in KBr.

The  $V_1$  centre is attributed to a hole trapped at a cation vacancy, and its band has a broad simple Gaussian form of bandwidth 0.7eV. There are indications, in the few alkali halides in which this centre has been studied, that the position of the  $V_1$  band is strongly characterised by the anion type (see Table IV (54)); not surprisingly, if Kanzig's (39) observations that the hole is localized on two of the anions bordering the cation vacancy are correct.

Not explicable as yet, is the triple nature of the band, if indeed the three peaks really are due to one centre. The electronic energy levels of the triatomic azide ion or radical will be of very different character to those of the monatomic halogen ion or atom, and it is not unreasonable to suppose that such differences will be reflected in the  $V_1$  centre in view of the strong dependence on anion type. Also crystal structure must have an effect since the B band of  $\text{NaN}_3$  is so very different and may be due to another kind of centre.

The increasing distinctness of the shoulders from  $\text{KN}_3$  and  $\text{CsN}_3$  can be attributed to the decreasing bandwidths of the component bands, an effect also noticeable in the A band. The shift to longer wavelength can be ascribed to an effect similar to that discussed for the A band.

(iii) C band. These bands were more difficult to study experimentally since they occurred in the "I.R." spectral region, use of which resulted in considerable bleaching. For this reason, they were plotted separately in figure 18, together with the times since the start of spectral recording; for  $\text{NaN}_3$  the band occurred more nearly in the "VIS", and was therefore plotted with the rest of the spectrum in figure 14. The position and shape of the C bands is much less certain than those of the other bands, since they are much weaker, and occur as shoulders on the long wavelength side of the A band. Approximate positions are:

$\text{NaN}_3$  740  $\mu$ ; 1.65 eV. Bandwidth 0.15eV

$\text{KN}_3$  790  $\mu$ ; 1.55 eV. (The different shape of the upper curve of figure 18 is attributed to bleaching effects).

$\text{RbN}_3$  820  $\mu$ ; 1.5 eV.

$\text{CsN}_3$  850  $\mu$ ; 1.45 eV. Very weak; rather doubtful.

Of the alkali halide models, the most likely to account for the C band is the  $F^{\prime}$  centre; the  $R_1$ ,  $R_2$  or M bands, which also occur in this region of the spectrum, are not found under the given experimental conditions. Even less has been published on the position of the  $F^{\prime}$  band than the  $V_1$  band; the only figure known to the writer being 730  $\mu$  for KCl, taken from a diagram in Seitz (16). That an  $F^{\prime}$  band should be formed, and that it should be weak, is quite likely if the designation of the A band as an F band is correct; for an  $F^{\prime}$  centre is formed by the capture of a conduction band electron by an F centre, and therefore, the number of  $F^{\prime}$  centres is always less than, and dependent on the number of F centres.

#### 4. Spectra of azides irradiated at room temperature.

Since there was no common structure to the spectra at room temperature, except for  $\text{RbN}_3$  and  $\text{CsN}_3$ , each azide will be considered separately.

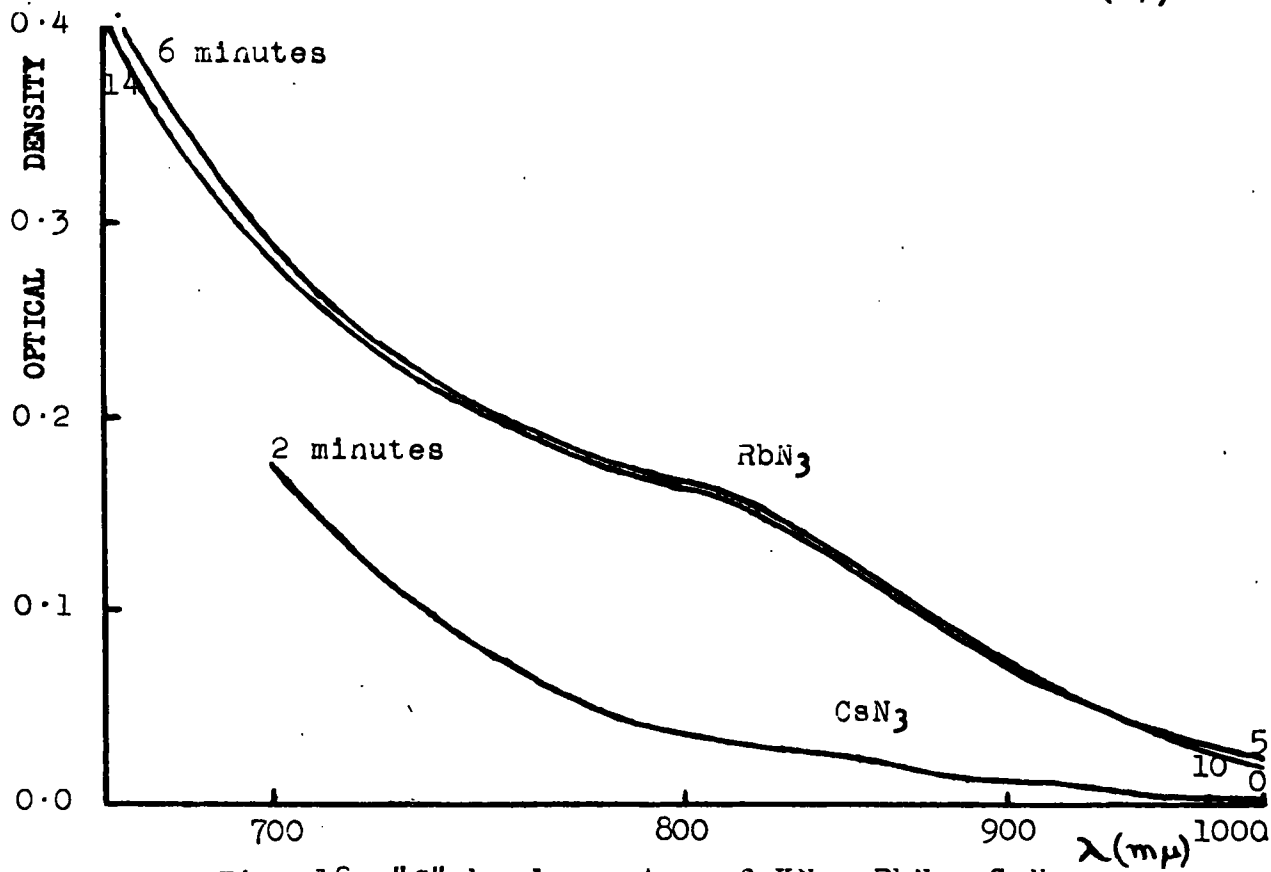
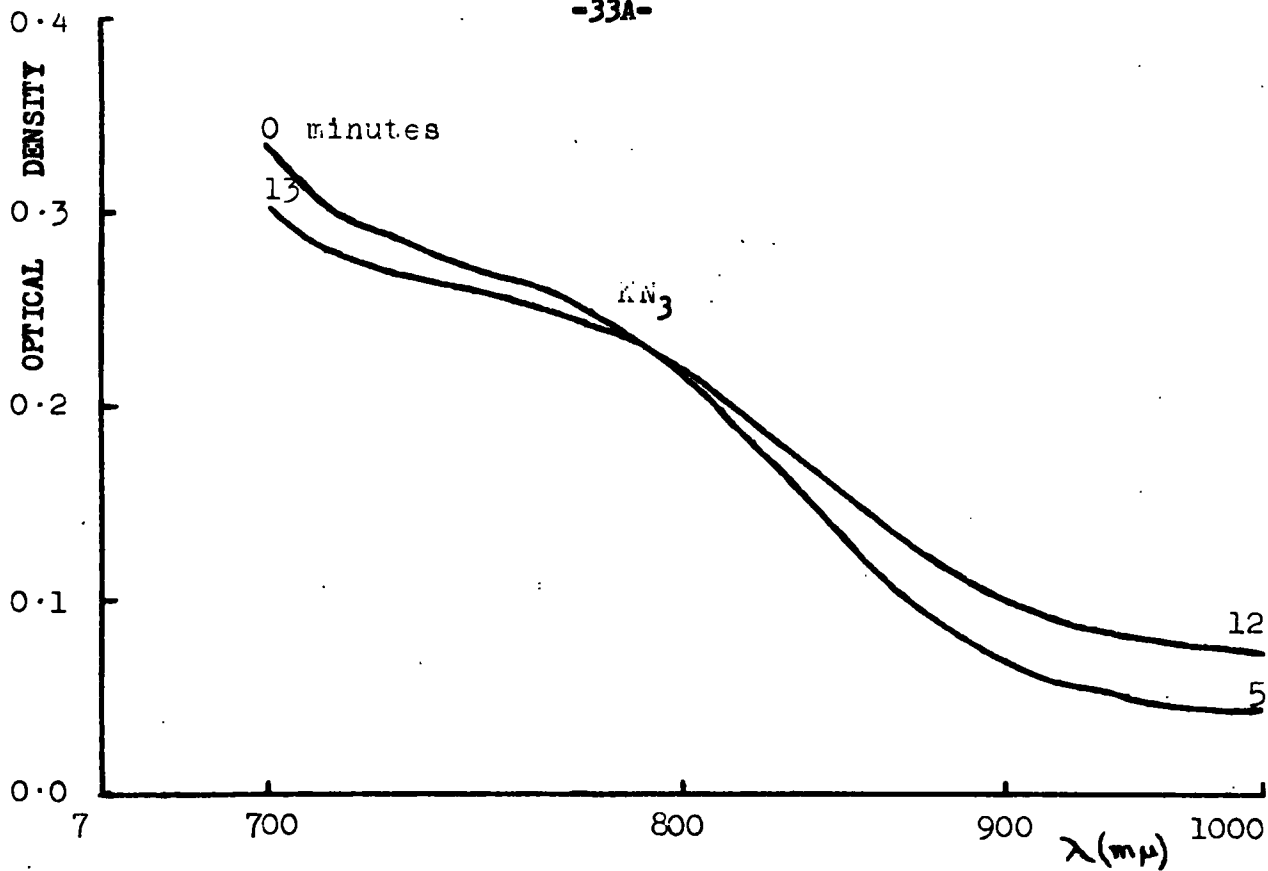


Fig. 18. "C" band spectra of  $\text{KN}_3$ ,  $\text{RbN}_3$ ,  $\text{CsN}_3$

(i) Sodium azide. The room temperature spectrum is given in figure 19I and consists of five bands; a broad strong band peaking at 342 mu (3.62 eV) of bandwidth about 1.4 eV, and four weak bands of approximately equal energy separation at about 560 mu (2.22 eV), 630 mu (1.97 eV), 730 mu (1.70 eV) and 860 mu (1.44 eV). There is some evidence to suggest that the latter four bands are associated since they were always observed together; further they disappeared together on standing at room temperature at the same time as the 342 mu band also decreased somewhat. Figure 14 IV shows the partially bleached A band of  $\text{NaN}_3$  with the 860 mu and 730 mu peaks on its long wavelength side; the others, if present, being masked by the A band. The 730 mu band may be present at lower temperatures in view of the slight kink in figure 14 II, but it is more reasonable to assume this is an unbleached portion of the 740 mu C band, since no attempt was made to bleach it completely. At room temperature, these four bands broaden so much that only two of them could be detected by Rosenwasser, Dreyfus and Levy(11) at 660 mu and 760 mu; the shift of the first peak is confirmed from figure 19 II. In marked contrast, is the behavior of the 342 mu band which is hardly affected by temperature changes.

A possible explanation of the four small peaks, accounting for their associated character, is that they are due to the electronic vibration spectrum of an unknown constituent, which could be an azide or impurity X-ray decomposition product (see further section 4(iii)). Such an entity would be susceptible to lattice vibrations thereby accounting for the broadening observed at room temperatures.

The 342 mu band is considered analogous to the 440 mu (2.82 eV) band of ultra-violet irradiated  $\text{KN}_3$  observed by Tompkins and Young (12) above 60°C, and ascribed by them to photoemission by potassium metal into the conduction band of the salt; the potassium metal being in the form of filaments and layers so that no colloid bands are observed. Assuming that the position of the conduction band is the same in both azides, the energy difference of

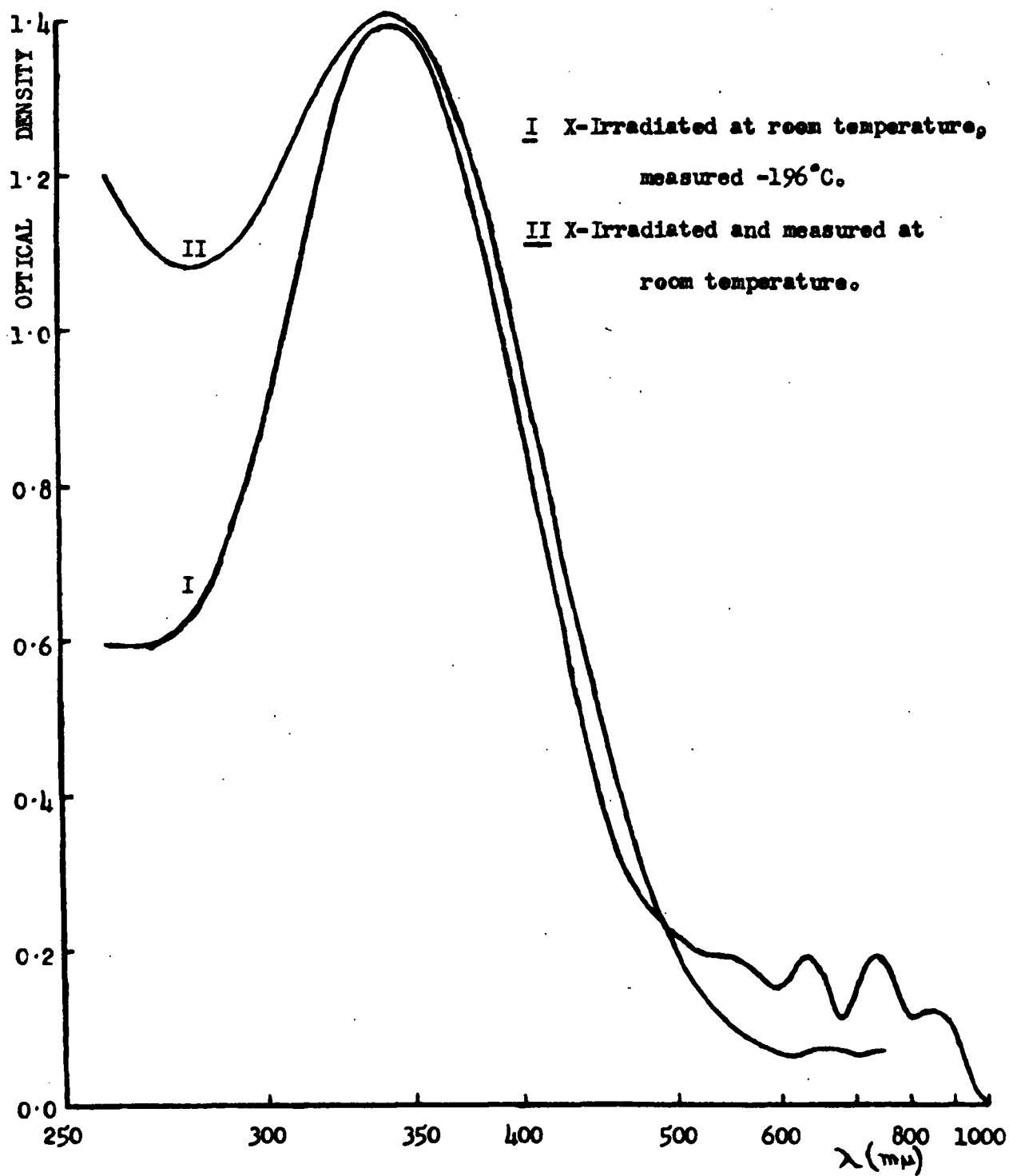


Fig. 19. Irradiated  $\text{NaN}_3$  spectra at room temperature.

the observed bands should be approximately equal to the difference in the ionisation potentials of the two metals, which is  $\sim 0.80 - 0.85$  eV. The observed energy difference is 0.80 eV in very good agreement. It should also be noted that Kaiser (56) using thin films of KCl condensed at room temperature, and containing excess sodium and potassium metal obtained similar bands at 335  $\mu$  (3.70 eV) and 438  $\mu$  (2.83 eV) giving an energy difference of 0.87 eV. Since the ionisation potential of the metal does not vary with temperature, the temperature invariance of the observed band can be explained on the assumption that the conduction band does not vary either. (On this basis, it is predicted that similar bands should be found in (heated)  $\text{RbN}_3$  and  $\text{CsN}_3$  at about 466  $\mu$  (2.66 eV) and 523  $\mu$  (2.37 eV)).

(ii) Potassium azide. The room temperature spectrum (figure 20) of  $\text{KN}_3$  consists of three peaks; a broad weak one at 340  $\mu$  not obvious in spectrum II, and two stronger ones at 590  $\mu$  and 760  $\mu$  of which the latter is the higher. Tompkins and Young (12) using U.V. irradiated  $\text{KN}_3$ , obtained a peak at 760  $\mu$  with structure at 550-570  $\mu$ , 725  $\mu$ , and 840  $\mu$ ; of the 550-570  $\mu$  shoulder they write:

"Unlike the main band, this shoulder is affected by temperature and is doubtless due to the presence of residual F-centres. On illumination at room temperature in the spectrophotometer with F-light for 2 min. this shoulder normally disappears with a resulting general increase in the (rest of the R') band, but in a minority of crystals shifts to 600  $\mu$ . This latter band is probably due to an impurity".

In the present work, no trace of the A band was obtained at room temperature for any azide, so "residual F-centres" are unlikely to be present under these conditions. The band at 600  $\mu$  may be the same as the experimental 590  $\mu$ ; there is no evidence to show that the latter is due to an impurity. The two strong experimental bands may be due to R centres; the Ivey (55)

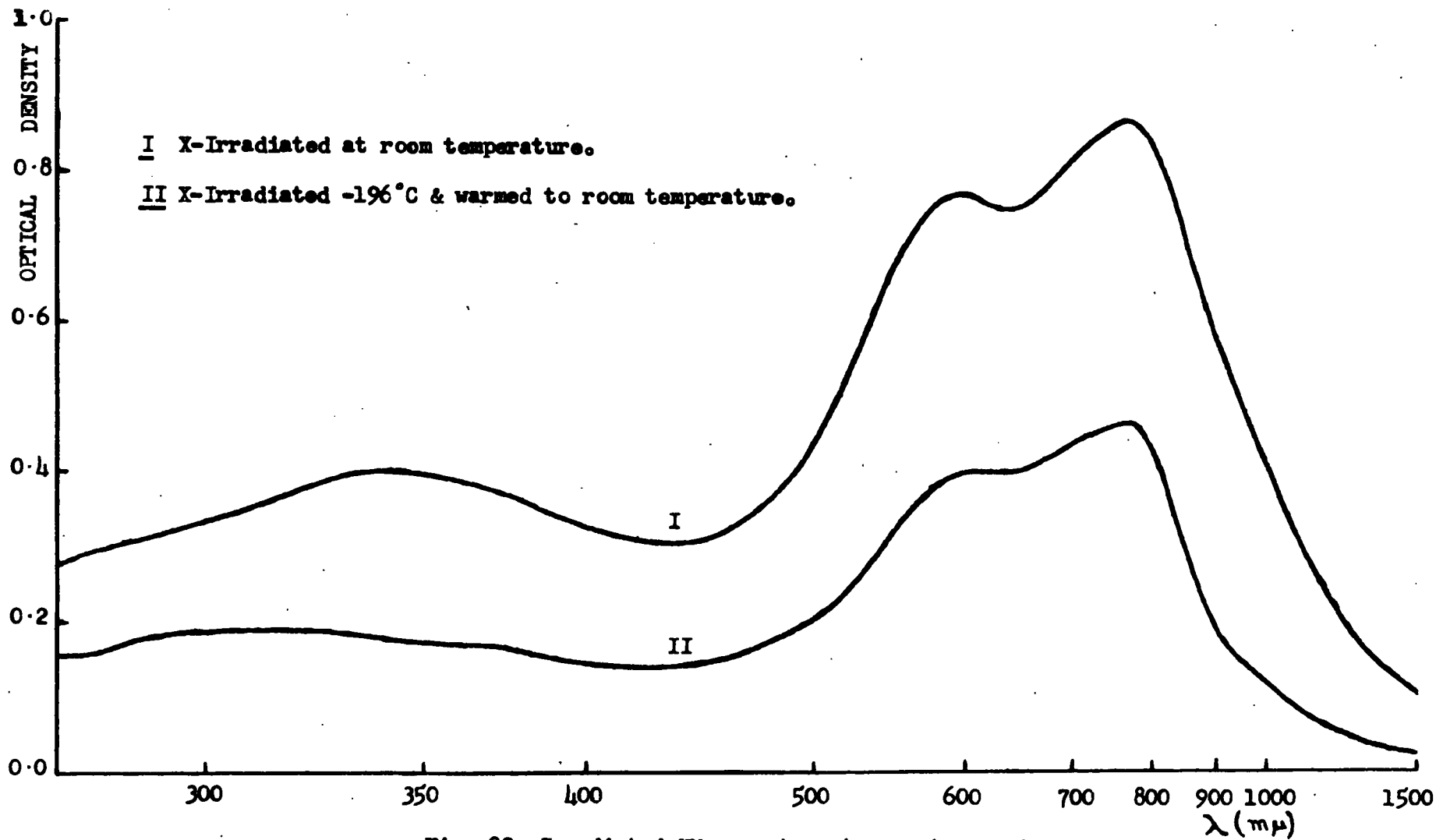


Fig. 20. Irradiated  $\text{KN}_3$  spectra at room temperature.

(Spectra measured at -196°C.)

formulas for the alkali halides are:

$$R_1 \quad \lambda_{\max} = 816 d^{1.84} \quad (A^\circ)$$

$$R_2 \quad \lambda_{\max} = 884 d^{1.84} \quad (A^\circ)$$

and for comparison,

$$F \quad \lambda_{\max} = 703 d^{1.84} \quad (A^\circ)$$

Ivey (55) attributes the similar powers to the fact that all these centres involve halogen vacancies only. Using the azide F centre formulas already obtained:

$$F \quad \lambda_{\max} = 3520 r_o^{0.38} \quad (A^\circ)$$

and multiplying by the appropriate factors 816/703 and 884/703:

$$R_1 \quad \lambda_{\max} = 4085 r_o^{0.38} \quad (A^\circ)$$

$$R_2 \quad \lambda_{\max} = 4430 r_o^{0.38} \quad (A^\circ)$$

For  $KN_3$ ,  $R_1 \lambda_{\max} = 659$  mu and  $R_2 = 714$  mu; not in agreement with the experimental bands. It should be pointed out that Ivey's formulae refer to room temperature, while the azide F band formula was calculated at liquid nitrogen temperature.

Tompkins and Young (12) attribute their 760 mu band, which varied markedly with the crystal, to that composite entity, the  $R'$  band, by analogy with the work of Scott (35) on KCl; they also tentatively ascribe, on kinetic data, a 760 mu band obtained by UV irradiation at liquid nitrogen temperature, to the M centre. It does not seem possible on the basis of the present data to reach any definite conclusions as to the nature of the 590 mu and 760 mu bands, except that they are most probably due to electron centres of the  $M, R$  type.

(iii) Rubidium and Caesium azides. The room temperature spectra (figure 21) of these two azides are qualitatively the same, and very different from that of  $KN_3$ . Both consist of a broad strong band in the ultraviolet, showing fine structure; the highest peaks occur at 330 mu and 375 mu respectively.

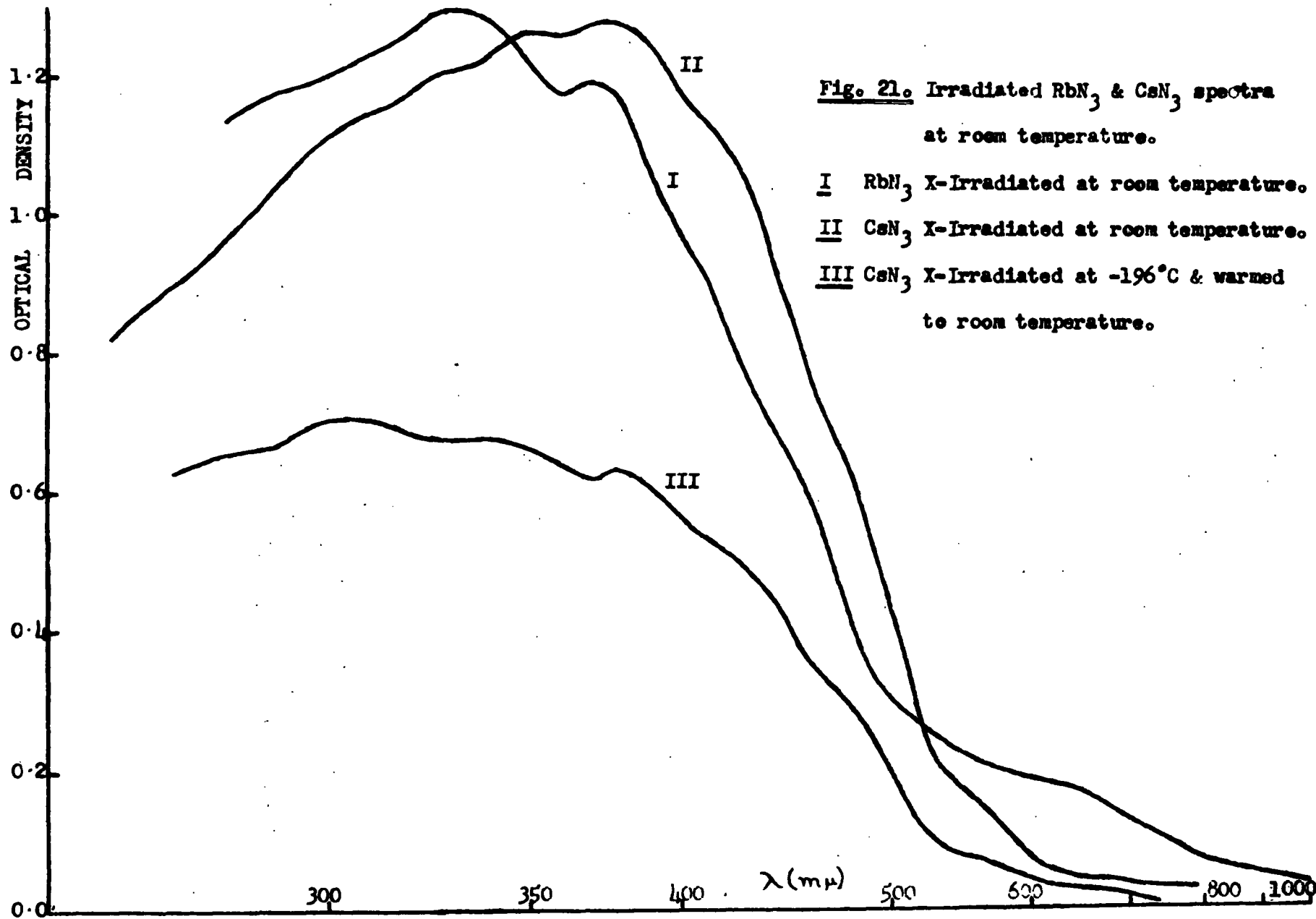


Fig. 21. Irradiated  $RbN_3$  &  $CsN_3$  spectra at room temperature.

I  $RbN_3$  X-Irradiated at room temperature.

II  $CsN_3$  X-Irradiated at room temperature.

III  $CsN_3$  X-Irradiated at  $-196^\circ C$  & warmed to room temperature.

Rubidium azide shows less fine structure than  $\text{CsN}_3$ ; bands occur at about 640, 455, 410, 370, 330 and (?) 290  $\mu$ , while for  $\text{CsN}_3$  bands about (?) 670, 560, 480, 430, 375, 350, 325 and 305  $\mu$  can be distinguished.

The fine structure can be assigned to a vibrational electronic transition, but it is questionable whether this is solely responsible for the observed absorption. It could be weak and superimposed on a broad strong band due to a V centre - presumably  $V_2$  or  $V_3$  since these are the only ones stable at room temperature in the alkali halides. However, both the  $V_2$  and  $V_3$  bands occur at short wavelengths very close to the first fundamental band; in particular their wavelength is much shorter than that of the  $V_1$  band. So if the assignation of the B band to a  $V_1$  centre is correct, the peaks around 330  $\mu$  and 375  $\mu$  are unlikely to be due to either of these centres. The absorption is not necessarily due to the same centre in the two azides, but the fact that the peak occurs at longer wavelengths in  $\text{CsN}_3$  makes this more probable.

The vibrational electronic transition postulated to account for the fine structure is difficult to explain except on impurity basis. The responsible agent must contain at least two atomic nuclei; some possible azide decomposition products fulfilling this condition are  $\text{N}_2^{n+}$ ,  $\text{N}_3^{n+}$ ,  $\text{N}_2$ ,  $\text{N}_3$  and  $\text{N}_6$ .  $\text{N}_2^+$  is a very energetic molecule requiring at least 15.8 eV for its formation from  $\text{N}_2$  (57); as such it is not likely to be formed on warming the  $\text{CsN}_3$  of figure 17 to room temperature. Similar considerations apply to  $\text{N}_2^{n+}$  and  $\text{N}_3^{n+}$ ;  $\text{N}_3$  corresponds to a positive hole, which would be trapped at a lattice defect to give a V centre, but the B band shows no such fine structure.  $\text{N}_6$  is equivalent to two positive holes, and would almost certainly decompose at once to give  $3\text{N}_2$ ; ordinary  $\text{N}_2$  would not absorb in the this spectral region. Triplet  $\text{N}_2$ , however, might absorb but would not be stable long enough to give an absorption spectrum (58); the same applies to triplet  $\text{N}_3^-$ .

Therefore the electronic vibrational transition is ascribed to impurities, of which the most probable are  $\text{OH}^-$  and  $\text{CO}_3^-$ .

References:

1. Allen, A.O., Effects of Radiation on Materials, U.S.A.E.C. leaflet #MDDC-962; May 20, 1947.
2. Heal, H.G., Can.J.Chem., 1953, 31, 1153.
3. Heal, H.G., Trans. Faraday Soc., 1957, 53, 210.
4. Wischin, A., Proc. Roy.Soc. A, 1939, 172, 314.
5. Thomas, J.G.N. and Tompkins, F.C., Proc. Roy. Soc. A, 1951, 210, 111.
6. Jacobs, P.W.M. and Tompkins, F.C., Proc.Roy.Soc. A, 1952, 215, 265.
7. Garner, W.E., and Maggs, J., Proc.Roy. Soc. A, 1939, 172, 299.
8. Thomas, J.G.N. and Tompkins, F.C., Proc.Roy. Soc. A, 1951, 209, 550.
9. Jacobs, P.W.M. and Tompkins, F.C., Proc. Roy. Soc. A, 1952, 215, 254.
10. Groocock, J.M., and Tompkins, F.C., Proc.Roy.Soc. A, 1954, 223, 267.
11. Rosenwasser, H., Dreyfus, R.W., and Levy, P.W., J.Chem.Phys., 1956, 24, 184.
12. Tompkins, F.C., and Young, D.A., Proc. Roy. Soc. A, 1956, 236, 10.
13. Goldstein, E., Zeits, F. Instrumentkunde., 1896, 16, 211. Quoted in reference (15).
14. Pohl, R.W., Proc. Phys. Soc., 1937, 49 (extra part), 4.
15. Seitz, F., Revs.Modern Phys., 1946, 18, 384.
16. Seitz, F., Revs. Modern Phys., 1954, 26, 7.
17. Inorganic Syntheses, Volume I, 78.
18. El-Shami, H.K. and Sherif, F.G., Egypt. J.Chem., 1958, 1, 35.
19. Audrieth, L.F., Chem. Revs., 1934, 15, 169.
20. Duval, C., Inorganic Thermogravimetric Analysis, Elsevier, 1953.
21. De Waard, R.H., Proc. Acad. Sci. Amsterdam, 1946, 49, 944.
22. Heal, H.G., Can.J.Chem., 1953, 31, 91.
23. Victoreen, J.A., J. App. Phys., 1949, 20, 1141.

24. Applied Physics Corporation, Instructions for Cary Recording Spectrophotometer, Sheet 4.
25. Lea, D.E., Actions of Radiations on Living Cells, C.U.P., 1946, page 12.
26. Frenkel, J., Zeits. Phys., 1926, 35, 652.
27. Schottky, W., and Wagner, C., Zeits. Phys. Chem. 1930, 11B, 163.
28. Mott, N.F., and Littleton, M.J., Trans.Faraday Soc., 1938, 34, 485.
29. Seitz, F., "Influence of Plastic Flow on the Electrical and Photographic Properties of the Alkali Halide Crystals", Symposium on the Plastic Deformation of Crystalline Solids, Mellon Institute, Pittsburg, May 1950, page 37.
30. Mott, N.F., and Gurney, R.W., Electronic Processes in Ionic Crystals, O.U.P. 1948, page 147.
31. Witt, H., Nachs. Akad. Wiss. Gottingen, 1952, 17. Quoted in Dekker, A.J., Solid State Physics, Prentice-Hall, 1957, page 381.
32. Duerig, H., and Markham, J., unpublished results, quoted in reference (16) page 9.
33. Mott, N.F., and Gurney, R.W., Electronic Processes in Ionic Crystals, O.U.P., 1948, page 114.
34. Pick, H., Ann. d. Physik, 1938, 31, 365.
35. Scott, A.B., Hrostowski, H.J., and Bupp, L.P., Phys.Rev., 1950, 79, 346.
36. Savostianova, M., Zeits. Physik, 1930, 64, 262.
37. Mie, G., Ann. Physik, 1908, 25, 377.
38. Casler, R., Pringsheim, P., and Yuster, F.H., J.Chem.Phys., 1950, 18, 887.
39. Kanzig, W., Phys. Rev., 1955, 99, 1890.
40. Dutton, D., and Maurer, R.J., Phys. Rev., 1953, 90, 126.
41. Hendricks, S.B., and Pauling, L., J. Am. Chem. Soc., 1925, 47, 2904.
42. Evans, B.L., and Yoffe, A.D., Proc. Roy. Soc. A., 1957, 238, 568.
43. Mott, N.F. and Gurney, R.W., Electronic processes in Ionic Crystals, O.U.P. 1948, page 100.

44. Isetti, G., and Neubert, T.J., J. Chem. Phys., 1957, 26, 337.
45. Debye, P., and Bueche, A.M., J. App. Phys., 1949, 20, 518.
46. von Hippel, A., Zeits. Phys., 1936, 101, 680.
47. Garner, W.E., Chemistry of the Solid State, London, Butterworths, 1955, page 61.
48. Højendahl, K., K. Dansk. Vidensk. Selsk. Math-fys. Medd., 1938, 16, 2, 133.
49. Gray, P., and Waddington, T.C., Proc. Roy. Soc. A., 1956, 235, 481.
50. Klemm, W., Zeits. Phys., 1933, 82, 529.
51. Tessman, J.R., Kahn, A.H. and Shockley, W., Phys.Rev., 1953, 92, 890.
52. Dreyfus, R.W., and Levy, P.W., Proc. Roy. Soc. A., 1958, 246, 233.
53. Mott, N.F., and Gurney, R.W., Electronic Processes in Ionic Crystals, O.U.P. 1948, page 98.
54. Landolt-Börnstein Tables, 6th Edition, 1954, I, 4, 981.
55. Ivey, H.F., Phys. Rev., 1947, 72, 341.
56. Kaiser, R., Zeits. Phys. 1952, 132, 482.
57. Frost, D.C., and McDowell, G.A., Proc. Roy. Soc. A., 1955, 232, 227.
58. Reid, C., Quart. Revs., 1958, 12, 205.